NTNU – Trondheim
Norwegian University of
Science and Technology

A Sensitivity Study of Ice Resistance Prediction Methods Using a Developed Bow Shape Modelling Tool

Sigrid Knutsdatter Gaup Aamot

Preface

This master thesis is a part of my Master of Science in Marine Systems Design carried out during the spring of 2015 at the Department of Marine Technology, Norwegian University of Science and Technology in Trondheim.

The purpose of this thesis was to perform a sensitivity analysis of reviewed ice resistance prediction methods with regard to the bow geometry and thereby to identify the knowledge gap and the limitations of the methods. In order to visualise and generate desired bow shapes, a parametric 3D model in MATLAB was developed.

The work of this thesis has been highly educational where I had a long learning process in MATLAB and I have gained useful knowledge about the study field in my thesis. The development of the parametric model took longer than initially planned and some changes were made to the objectives during the work of this thesis.

I wish to express my gratitude to my supervisor Professor Sören Ehlers for helpful guidance and great support throughout the work of this thesis. Further, I would like to thank PhD-candidate Sandro Erceg for his appreciated input and support. In addition, I wish to thank postdoc researcher Henry Piehl at the Department of Marine Technology who has been very helpful throughout the modeling in MATLAB. Last but no least, my office for support during the work and good working environment.

<div align="center">

Trondheim, June 10, 2015

Sigrid Knutsdatter Gaup Aamot

</div>

ii

Abstract

The shipping in ice-covered waters increases the need of knowledge and understanding about physical effects of the icebreaking process during the ship-ice interaction. The shape of the ship bow will affect the ice resistance significantly and thus it is important to consider its geometry when predicting the ice resistance. The ice resistance on ships advancing in level ice can be predicted by either performing model tests or applying methods estimating the ice resistance.

The aim of this thesis is to perform a sensitivity analysis of chosen ice resistance prediction methods with regard to the bow shape and thus identify the effect of the bow geometry on the breaking resistance. The desired bow shapes are generated through a parametric 3D model developed in MATLAB.

The parametric 3D model is built up by a "bow skeleton" which consists of a mesh grid with connected control points that depend on bow length, ship beam, ice thickness and five angles describing the bow shape. To obtain a 3D bow shape, a surface was added made up by non-uniform rational basis splines. By adjusting the control points, a desired bow shape can be generated. For simplicity, the model is only considering the ice belt area.

A sensitivity analysis was performed on the methods of Lindqvist (1989) and Erceg et al. (2014) with regard to the bow geometry as they both are considering the same parameters describing the bow shape angles, and the methods are decomposing the ice resistance to be able to estimate the resistance components separately. The method of Lindqvist was found to be more sensitive to larger buttock angles and smaller waterline entrance angles, with regard to the increased relative breaking resistance. However, overall the method seems to be more sensitive to a change of the buttock angle as the relative breaking resistance would increase significant in line with the increase of the buttock angle. A decreased flare angle is found to give smaller breaking resistance, and the change of ship beam will not have a significant effect on the breaking resistance. Thereby, the smallest breaking resistance will be found for a large waterline entrance angle and a small buttock angle, which can be recognised as the spoon-shaped bow.

The method of Erceg was found to show a similar results, which means that a small waterline entrance angle and large buttock angle will result in a larger breaking resistance. The parametric model was found to be limited to bow shapes with average waterline entrance angles up to 45 degrees and average buttock angles up to 60 degrees, which excludes landing craft bows. The method of Erceg seemed to be limited for waterline entrance angles ranging from 20 to 50 degrees, and buttock angles from 20 to 45 degrees, with regard to the implemented parametric model.

iv

Sammendrag

Den økte skipstrafikken i islagte farvann øker behovet for kunnskap og forståelse av de fysiske virkningene av den isbrytende prosessen under interaksjonen mellom skip og is. Formen på skipets baug vil påvirke ismotstanden betydelig, og dermed er det viktig å vurdere dens geometri når en skal forutsi ismotstanden. Ismotstanden på skip som opererer i is kan bli forutsett ved enten å utføre modellforsøk eller anvender metoder som kan estimere ismotstanden.

Målet med denne oppgaven er å utføre en sensitivitetsanalyse av utvalgte metoder for prediksjon av ismotstand med hensyn til baugprofilen og dermed identifisere effekten av geometrien av baugen på motstanden generert under isbrytingen. Baugprofilene vil bli generert ved bruk av en parametrisk 3D-modell utviklet i MATLAB.

Den parametriske 3D-modellen er bygget opp av et "baugskjelett" som består av et gitter med tilkoblede kontrollpunkter som er avhengige av baugens lengde, skipets bredde, istykkelse og fem vinkler som beskriver baugprofilen. For å oppnå en 3D-baugprofil, ble det lagt til en overflate som består av "non-uniform rational basis splines". Man kan generere en ønsket baugprofil ved å justere kontrollpunkten. For enkelhetsskyld vil modellen kun betrakte området for isbeltet.

En sensitivitetsanalyse ble utført på metoder fra Lindqvist (1989) og Erceg et al. (2014) med hensyn til baugens geometri siden begge vurderer de samme parameterene som beskriver vinklene i baugprofilen, og metodene dekomponerer ismotstanden slik at motstandskomponentene kan beregnes separat. Metoden av Lindqvist virker å være mer følsom for en endring i baugvinklene for større endevinkler og mindre vannlinjeninngangsvinkler, med hensyn til økningen i den relative brytemotstanden. Likevel virker metoden til å være mer følsom for en endring i endevinkelen siden den relative brytemotstanden vil øke betydelig i takt med økningen av endevinkelen. En redusert utspredningsvinkel vil gi mindre brytningsmotstand, og endring av bredden på skipet vil ikke gi en betydelig effekt på brytningsmotstanden. Dermed vil den minste brytningsmotstanden bli funnet for en stor vannlinjeninngangsvinkel og en liten endevinkel, noe som kan gjenkjennes som en skjeformet baug.

Metoden fra Erceg viser seg å resultere i en lignende tendens, noe som betyr at en liten vannlinjeinngangsvinkel og stor endevinkel vil resultere i en større brytningsmotstand. Den parametriske modellen er begrenset til baugprofiler med gjennomsnittlige vannlinjeninngangsvinkler for opp til 45 grader og gjennomsnittlige endevinkler for opp til 60 grader, noe som utelukker landgangsformet baugprofiler. Metoden til Erceg virker å være begrenset til baugprofiler med vannlinjeinngangsvinkler fra 20 til 50 grader, og endevinkler fra 20 til 45 grader, med hensyn til den implementerte parametriske modellen.

Contents

List of Figures

List of Tables

Nomenclature

Symbol	Description
α	Waterline entrance angle
α_1	Waterline entrance angle at stem in parametric 3D model
α_2	Waterline entrance angle at exit in parametric 3D model
β	Angle between ship longitudinal axis and each individual ice beam
β_1	Frame angle 1
β_2	Frame angle 2
β_{avg}, ϕ_{avg}	Average buttock angle in bow region
ϕ	Buttock angle
ϕ_1	Additional buttock angle 1 in parametric model
ϕ_2	Additional buttock angle 2 in parametric model
ϕ_3	Additional buttock angle 3 in parametric model
φ	Buttock angle at stem
γ	Average flare angle in bow region
ψ	Flare angle
μ	Friction coefficient
ν	Poission coefficient
$\sigma, \sigma_b, \sigma_f$	Flexural strength of ice
ρ_i	Ice density
ρ_w	Salt water density
$\Delta\rho$	Density difference between ice and water
B	Ship beam
C_1, C_2, C_3	Empirical coefficients in the method of Enkvist (1972)
C_B, C_S, C_V	Empirical values in the method of Vance (1975)
C_H	Hull condition factor
C_s	Salinity factor for water
D	Average breaking depth
D_p	Propeller diameter
E	Young's elastic modulus of ice
f_1, f_2, f_3, f_4	Constants in the method of Riska et al. (1997)
F_v	Vertical force acting on ice from stem
g_1, g_2, g_3, g_4	Constants in the method of Riska et al. (1997)
g	Gravitational constant
H_1	Height from z=0 to ice bottom surface
H_2	Height from waterline to top of bow
H_3	Height from z=0 to top of bow
H_4	Height from z=0 to bottom of bow
h_i	Ice thickness
H_s	Snow layer thickness
k_1, k_2, k_3, k_4, k_5	Empirical coefficients in the method of Kashteljan et al. (1969)
L, L_{pp}	Ship length between perpendiculars

Symbol	Description
L_{bow}	Length of bow
L_{oa}	Ship length over all
L_{par}	Length of parallel midbody
P_D	Propulsion power
T	Ship draught
t	Surface temperature of ice or air temperature
T_b	"Draught", height from z=0 to waterline
v	Ship speed
v_{ow}	Ship speed in open-water
W	Width of ice cusps

1. Introduction

1.1 Background and Motivation

The increased activity in shipping and exploration for hydrocarbons in ice-covered waters demands a market of icebreakers and ice-capable vessels. Icebreakers and ice-capable vessels are required of having a well-functioning machinery and a propulsion system that can handle ice and cold temperatures. The ship hull has to be designed to achieve low ice resistance in a continuous icebreaking process and at the same time maintain good ship performance. The bow shape area of a ship hull is of utmost importance in the icebreaking process and a well-shaped bow designed for handling ice loads should break the ice in an efficient way while obtaining low ice resistance values. The angles describing the bow shape are therefore seen as some of the most important parameters when evaluating the ice resistance.

Semi-empirical and numerical methods for ice resistance prediction are developed over the past decades in order to estimate the forces acting on the ship hull advancing in level ice, and thereby give an indication of the ship performance in certain ice conditions. The methods are applied in an early design phase to predict the ice resistance instead of performing model tests, which are more reliable, but costly. The non-homogeneous properties of ice makes it difficult to measure and predict ice conditions and thus the methods of ice resistance prediction are under constant development in order to find the most reliable and applicable method. The existing methods are based on diverse assumptions and will therefore limit the applicabilities of the methods. Hence, there is a need of methods that are applicable for all ice conditions and ships with different main dimensions and bow shapes.

In this master thesis, a review of the historical development of icebreakers and the hull design of icebreakers with focus on the bow area are presented. In addition, this thesis deals with a review of the existing semi-empirical and numerical ice resistance predictions methods to identify the knowledge gaps. The main purpose of this thesis is therefore to identify the knowledges gap among selected methodologies for ice resistance prediction and to identify how sensitive the methodologies are towards a change in the bow geometry. In order to do so, a sensitivity analysis has to be performed with regard to the bow geometry by adjusting the bow shape angles and thereby also identify applicability and uncertainties related to the applied methods. The methods to be compared are based on common parameters describing the bow geometry, and they should include a decomposing of the ice resistance in order to be able to consider one resistance component at time, which in this case will be the breaking resistance.

By investigating the effect of the bow geometry on the ice resistance during an icebreaking process, the combination of bow angles resulting in a minimum breaking resistance can be found. The bow angles found to be resulting in the lowest ice resistance for each method, will be compared against existing icebreaking bows, and the results of the methods will be analysed and discussed. To visualise and generate desired bow shapes, a parametric 3D model will be developed in the program MATLAB. The model will be based on parameters representing the bow geometry and the ice thickness of an incoming ice edge during the ship-ice interaction. The model can thereby be used in a simulation procedure of a ship advancing in level ice to identify the physics of the icebreaking process, and to observe how the bow geometry will affect the breaking of the ice edge. Hence, the instantaneous ice loads acting on the bow in certain ice conditions can be measured.

1.2   Objectives

The main objectives of this master thesis are:

- To perform a literature review with focus on existing semi-empirical and numerical methods for ice resistance prediction in order to identify knowledge gaps, and to compare the methods with regard to considered parameters;

- To select methods suited for sensitivity analysis, which are chosen based on common parameters describing the bow geometry and which can be applied to estimate the breaking resistance;

- To apply the selected methods for different bow shapes in order to identify the effect of the bow geometry on the breaking resistance, and to find the combinations of bow shape angles resulting in the lowest breaking resistance;

- To develop a parametric 3D bow model in MATLAB considering parameters describing the bow geometry in order to generate desired bow shapes where the model will account for full curvature in all directions;

- To compare and discuss the obtained bow shapes for each method with existing icebreaking bow shapes, and thereby discuss limitations and uncertainties related to the applied methodologies, including the parametric model.

1.3   Scope of Work and Limitations

The literature study will be limited to chosen semi-empirical and numerical methods for ice resistance predictions for ships advancing in level ice, and the modeling of the bow shapes will be done by using the program MATLAB. Furthermore, this thesis will focus on the bow shape without considering rest of the ship hull.

The methods developed for ice resistance prediction are considering the hull-ice interaction to compute ice resistance, where the contact area is between the ice belt of the ship and the ice edge. Due to this, and for simplicity, the ice belt region will be the considered area in

the parametric model developed in MATLAB, which means that the top and the bottom of the bow will be disregarded. In addition, the main focus will be set towards the breaking component of ice resistance.

The sensitivity study will only be limited to the effect of the bow geometry on the breaking resistance, and thus results related to ice properties and ice thickness are out of scope in this thesis.

1.4   Thesis Outline

This thesis consists of the following chapters:

After an introduction of the master thesis in **Chapter 1** concerning background, motivation, objectives, scope and limitations, **Chapter 2** presents state of the art of this thesis. The state of the art includes literature study where the interaction process between ship hull and ice is described, together with a historical review of icebreakers, and it presents the characteristic design of icebreaking bows. In addition, semi-empirical and numerical methods for ice resistance prediction are presented, compared and discussed in this chapter in order to find suitable methods to apply in the sensitivity analysis.

Chapter 3 describes the developed parametric 3D bow model in MATLAB which generates desired bow shapes. The steps of the modelling process is explained in a flow chart and the main file developed in MATLAB is thoroughly explained.

Chapter 4 presents a sensitivity analysis of selected methods with regard to the bow geometry, and the results obtained from the methods are compared and discussed.

Chapter 5 presents the discussion and conclusion of this thesis, while the last chapter, **Chapter 6** presents recommendations and suggestions for further work.

2. Literature Study

2.1 The Interaction between Ship Hull and Ice

When a ship is transiting in ice-covered water, there will be ice resistance on the hull due to the ship-ice interaction. The ice resistance depends on the ship's ability to break and displace the ice, and the ice resistance can be divided into three main force components according to Riska (2011a): breaking forces, submergence forces and sliding forces. The breaking forces are related to the moment where the ice is breaking, which includes crushing, bending and turning of ice and the submergence forces are related to the submerging of ice floes. The sliding forces will include the frictional forces between ship hull and ice and due to the frictional forces, the ice resistance will be speed dependent (Riska, 2011a,b).

In the ship-ice interaction, the first process that will happen is local crushing of the ice edge at the stem of the bow, and after the bow penetration of the ice edge, there will occur crushing of ice against the hull. The crushing force in the icebreaking process will increase with an increasing contact area until the vertical component of the force is large enough to make the ice bend due to a bending moment occurring in the ice cover. When the bending moment is larger than the bending strength of the ice, crack formations in the ice will be induced and ice floes will break off the ice covers, and the process is repeated in each contact point between the ship hull and the ice edge. The ice floes will thereafter go through a turning process until they are parallel with the ship hull before the floes are submerged. The ice floes will then slide along the hull until they are directed away from the hull (Riska, 2011b; Su et al., 2010).

The ice loads acting on a ship hull are under no circumstances uniform, and this can be identified by observing and measuring the breaking pattern in level ice which is created when ice floes are breaking off from the intact ice sheet. By observing and measuring the breaking pattern, crushing and breaking of ice in the bow area can be discovered. The measurements of the ice loads acting on the bow can be identified during a time period and due to this, the ice resistance can be found (Riska, 2011a). An illustration of the ice load acting on one single frame at the bow in a given period of time is illustrated in Figure 2.1. Each peak illustrates bending failure of the ice, which means ice floes that are breaking off from the ice cover (Riska, 2011b). It can be seen from Figure 2.1 that there will be several peaks in a short amount of time and a high amount of irregularities. The ice loads acting on the bow are constantly changing and the breaking pattern will be irregular. This can be explained by the non-homogenous properties of the ice. Due to this, it is difficult to predict ice resistance and to predict exactly how and when the ice will fail.
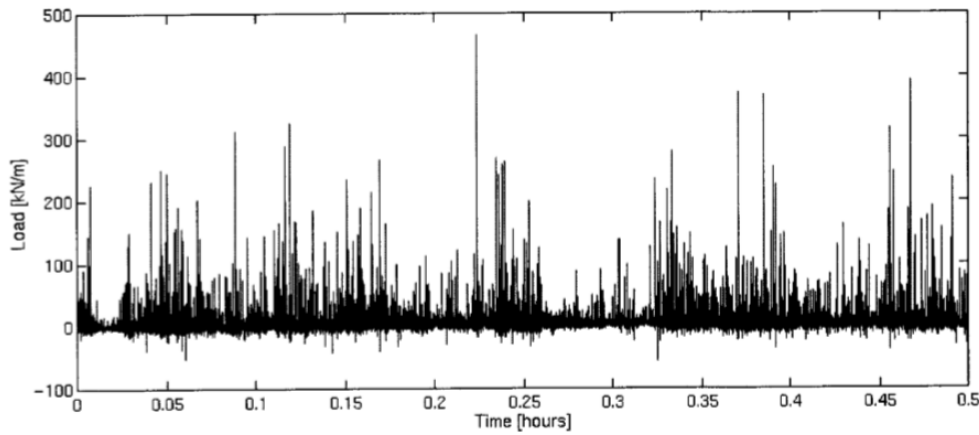
Figure 2.1: Ice load acting on one frame at the bow during a period of time (Riska, 2011b).

In water there will be no resistance when there is no forward speed, but in ice there will be resistance that has to be accounted for when the ship speed is equal to zero. If the ship should be able to move forward in ice, the propeller thrust has to overcome this ice resistance. Due to this, the ice resistance at zero forward speed is higher compared to ice resistance at low speed, and the ice resistance can be seen as approximately linear with ship speed (Riska et al., 1997). When the ship has a very low speed, there will be a point where the ice resistance will be higher than the thrust, and therefore bring the ship to a stop. Due to this, a ship has to maintain a minimum speed to be able to proceed in ice.

The ice resistance components depend on the ice conditions, such as level ice or brash ice, and thus the magnitude of the components will vary. The total ice resistance is given as summation of open water resistance and ice resistance, where ice resistance consists of breaking, submersion and friction resistance. The breaking resistance depends on bow shape, ice thickness and ice strength, while the submersion resistance will vary with the bow shape and ice thickness, and the friction resistance will depend on the hull form, speed and thickness of ice and snow (Kjerstad, nd). The ice resistance can be found from full-scale measurements during ice trials, by model tests or by application of semi-empirical and numerical ice prediction resistance methods, which are applied in an early design phase to indicate the ice resistance for different ice conditions. The methods are based on diverse assumptions, which will limit the applicability of the considered method and also the capability to predict the ice resistance. There are suggested many different formulations to estimate the ice resistance and some of the existing ice resistance prediction methods will be presented in Section 2.5 and 2.7.

2.2   Ship Performance in Level Ice

Ship performance in ice is evaluated by the ships icebreaking and ice-manoeuvring abilities where the icebreaking ability depends on how thick ice the ship can break through in forward speed. The speed that a ship can attain in ice depends on the ice resistance, which again depends on several factors such as ice properties, hull shape, main dimensions and propulsion

(Riska, 2011a). The performance in level ice can thus be indicated by ice thickness versus ship velocity curve. To determine the plots in the diagram, the curve for ice resistance versus ship velocity has to be determined first, which will vary with the ice thickness. Furthermore, the net thrust to overcome the ice resistance has to be estimated by applying Equation (2.1) from Riska (2011a):

$$T_{NET} = T_B \cdot (1 - \frac{1}{3}\frac{v}{v_{ow}} - \frac{2}{3}(\frac{v}{v_{ow}})^2) = K \cdot (P_D \cdot D_P)^{\frac{2}{3}} \cdot (1 - \frac{1}{3}\frac{v}{v_{ow}} - \frac{2}{3}(\frac{v}{v_{ow}})^2) \qquad (2.1)$$

where T_B is bollard pull expressed as $K \cdot (P_D \cdot D_P)^{\frac{2}{3}}$, where K is an empirical factor (0.78 for single screw and 0.98 for double screw ships), P_D is propulsion power, D_P is propeller diameter, v is the ship speed in ice and v_{ow} is the open water speed. In this thesis, the focus will not be towards the ship performance, but rather towards the ice resistance due to different bow shapes with main focus on the breaking component.

2.3 Historical Review of the Design of Icebreakers and Ice-capable Ships

The design of icebreakers and ice-capable ships goes all the way back to the middle of 18th century where the main events of the historical development of the design takes place. The ships have developed through the years based on experience and knowledge and around the 1830's the first icebreaking ships were designed, but the dedicated icebreakers came between 1860 and 1900 (Riska, 2011a).

The first steam-powered icebreaker was built in 1864, the Russian Pilot. Pilot was designed to slide on to the ice and break it, and to clear the ice away from the hull (Institution, 2007). The design of Pilot was later adapted to the German ship Eisbrecher Eins in 1871, which had a spoon-shaped bow instead of a sharp bow, just like Pilot. The rounded bow made it possible for the ship to rise up on the ice and break the ice from the top with its weight.

Another well-known and recognized ship was Fram, which was built in 1893 for the polar expeditions of Fritjof Nansen (Morley, 1962). Fram was designed to be forced up on the ice due to the rounded hull instead of resisting the ice loads, which can be seen as a quite unique design (Kjerstad, nd). However, the first modern and dedicated polar icebreaker in the world was the Russian Yermak in 1899 (Kjerstad, nd; Morley, 1962) which had a small stem angle and a design based on the design of Pilot.

The icebreakers that were designed in the 19th century is described thoroughly by Riska (2011a). The design consisted of a very small buttock line angle, φ, at the stem (the stem angle), and the buttock lines and the waterlines were rounded. The sides had a small inclination (defined by β), while the flare angle, ψ, was aimed to be as small as possible. The different angles can be seen in Figure 2.2.
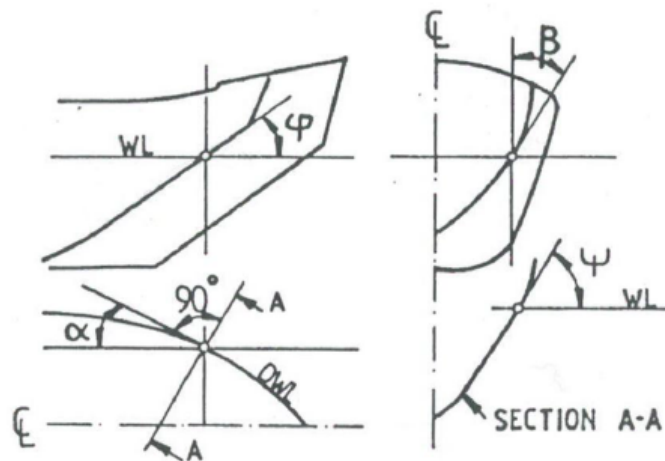
Figure 2.2: Hull angles on an icebreaking bow (Riska, 2011a).

An event that has made a considerable impact on the bow shape of modern icebreakers, was the proposed bow form for polar icebreakers, so called the White bow, which has a concave form with small stem angle. The bow was designed to improve the continuous icebreaking and the ramming and extraction ability (Jones, 2004). This was done by designing a blunter bow, decrease the friction coefficient and increase the thrust.

In the later years, more innovative designs for icebreakers are produced. An example of this is the Swedish icebreaker Oden constructed in 1988. The ship has a shape like a flat-bottomed skiff, a flat landing craft bow, which allows the ship to ride up on the ice and break the ice by its weight (Institution, nd). Another innovative design was released by Aker Arctic in 2013, an asymmetrical icebreaker, which is illustrated in Figure 2.3. The design is quite different from previous designs, and it is based on the DAS design. The icebreaker can operate efficiently ahead, astern and obliquely sideways due to azimuth thrusters place. The benefits of the design are excellent steering capabilities, in terms of being able to move in any direction in different ice conditions, such as ice ridges (Pospiech, 2013).
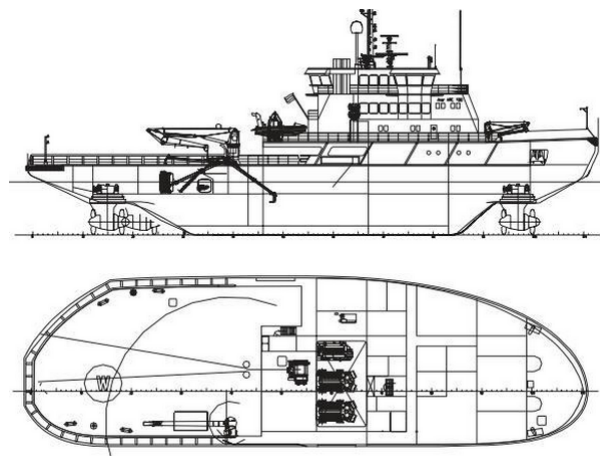
Figure 2.3: Asymmetrical icebreaker designed by Aker Arctic (Pospiech, 2013).

2.4 Characterisation of Icebreaking Bow Shapes

2.4.1 Main Features of an Icebreaking Bow

The typical bow shape of icebreakers is shown in Figure 2.4. The top of Figure 2.4 illustrates the typical characteristics of an icebreaking bow, while the bottom of the figure illustrates the bow shape of a modern icebreaker. A modern icebreaker has a rounded stem, which will reduce the crushing at the stem, and buttock lines that ice floes will follow. The bow plough will push the ice floes to the side rather than letting the floes get under the ship. However, the disadvantage of a plough is an increase in total resistance. Another important aspect with the bow shape of an icebreaker is the flare angle which will contribute to improved icebreaking and submergence of ice blocks. The bow shape angels are related to each other and thus the buttock angle will also contribute to efficient icebreaking and ice submergence (Sodhi, 1995). The stem angle will bend the ice and break it efficiently if the angle is sufficiently small, and thus reduce the crushing. A small stem angle will induce a larger bending force and at the same time keep the horizontal component small. Due to this, the stem angle is normally 20°-25° degrees for icebreakers. The last angle that is of importance regarding the bow shape is the waterline angle, which will contribute to clearing efficiency (Sodhi, 1995).
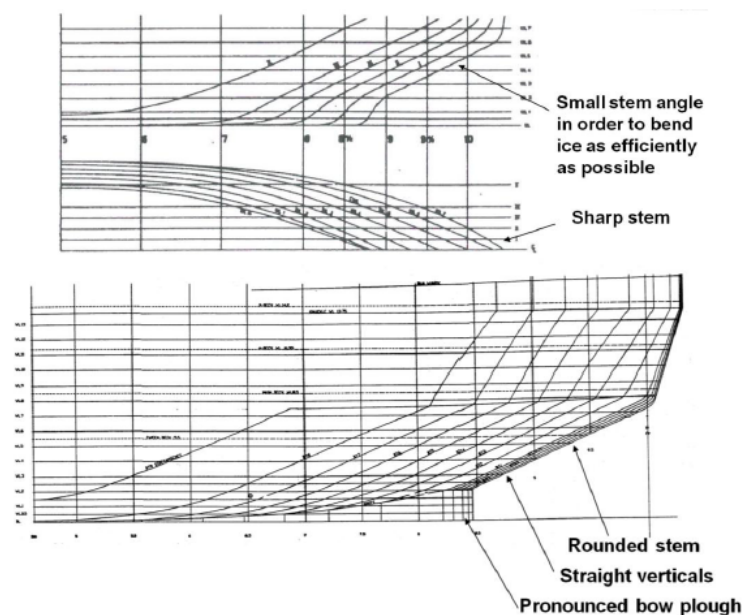
Figure 2.4: Top: Typical icebreaking bow. Bottom: Modern icebreaker (Riska, 2011a).

It can be seen from Figure 2.4 that the typical bow shapes doe not have any bulb. The bulb will not break ice in an efficient way, but a non-bulbous bow will have disadvantages in open water as the open water resistance will increase.

In addition to the bow shape angles, the ship beam will contribute to an impact on the ice resistance according to Riska (2011a). A greater beam will give an increased ice resistance, yet an icebreaker escorting a vessel should not be narrower than the escorted vessel. If the bow of the ship breaks a smaller channel than the beam of the ship, shoulder crushing may

occur. Shoulder crushing should be avoided as it will increase the ice resistance significantly and the ship hull will be further exposed to frictional wear.

2.4.2 Existing Bow Shapes

The characterisation of the bow shapes of commercial icebreakers today has changed and improved over decades, but the bow shapes still have some similarities to the early design of icebreakers. The bow shape of an icebreaker is characterized by the angles shown in Figure 2.2. The design of the bow shapes today has increased flare angle, and reduced waterline angles, stem and buttock angles compared to earlier designs. Figure 2.5 from Sodhi (1995) illustrates seven bow shapes that have been applied to icebreakers.
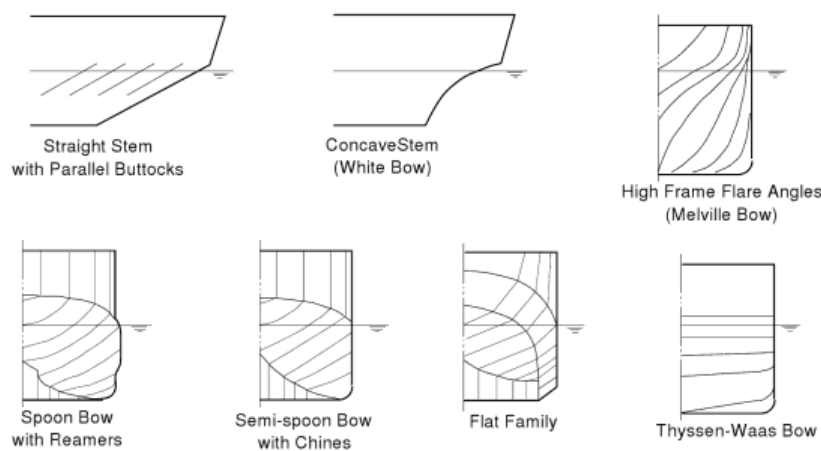
Figure 2.5: Types of icebreaking bows (Sodhi, 1995).

The first bow shape, straight stem with parallel buttocks, has been used in Russian and Finnish icebreakers since around the middle of 19th century, while the concave bow stem was used on icebreakers from the 1970s to 1984. The Melville bow, was developed to reduce the ice resistance by reducing the icebreaking component. The spoon bow with reamers and the semi-spoon bow with chines have both increased open-water resistance, but they improved icebreaking performance. The flat family bow shape is similar to the spoon-shaped bow, but it was designed to save construction costs. The last bow shape in Figure 2.5, is the Thyssen-Waas bow (also called flat landing craft bow), which is quite different from the other bow shapes as it is characterized by flat waterlines and extended beam, low stem angle and high flare angles under the waterline (Sodhi, 1995).

2.5 Semi-Empirical Methods for Ice Resistance Prediction

This section will emphasise suggested semi-empirical formulations for ice resistance prediction presented by Kashteljan et al. (1969), Enkvist (1972), Vance (1975), Lindqvist (1989), Keinonen et al. (1991, 1996) and Riska et al. (1997). In the end of the section, a comparison of the different formulations will be presented with regard to considered parameters and validation against full-scale measurements.

2.5.1 Kashteljan et al. (1968), Enkvist (1972) and Vance (1975)

A historical review of the ship performance is presented from 1888 to 2004 in the paper of Jones (2004), "Ships In Ice - A Review", which includes suggested formulations for calculating ice resistance. However, the main focus will be towards the development after the 1960s, when significant events took place which had major impacts on the development of the icebreaker design, such as the Arctic voyage of Manhattan in 1969 and rise in oil prices in 1973 and 1979.

Kashteljan et al. (1969) were one of the first to break the ice resistance into components according to Jones (2004), and they developed a formulation based on model testing anf full-scale measurements of the icebreaker Yermak. The equation is given as

$$R_{tot} = k_1 \mu_o B \sigma h_i + k_2 \mu_o \rho_i h_i^2 + k_3 \frac{1}{\theta_2} B^{k_4} v^{k_5} \tag{2.2}$$

where k_1, k_2, k_3, k_4 and k_5 are coefficients determined by experiments, μ_o and θ_2 are related to Shimansky's ice cutting parameters, B is ship beam, σ is ice strength, h_i is ice thickness, ρ_i is density of ice and v is ship speed. The first term is describing resistance due to icebreaking, the second term describes resistance due to forces connected with weight, and the last term is resistance due to passage through broken ice.

Another important contributor to the knowledge of ship performance in level ice is the semi-empirical formulation derived by Enkvist (1972). The ice resistance is given by the following equation

$$R_{tot} = C_1 B h_i \sigma + C_2 B h_i T \rho_\Delta g + C_3 B h_i \rho_i v^2 \tag{2.3}$$

where C_1, C_2 and C_3 are empirical coefficients, T is ship draft, ρ_Δ is $\rho_w - \rho_i$ (ρ_w is density of water), and g is the gravitational acceleration constant. The equation of Enkvist (1972) was validated by comparing the results with full-scale data from three ships.

Vance (1975) developed an equation for ice resistance based on model and full-scale data from five ships. The equation is given as

$$R_{ice} = C_S \rho_\Delta g B h_i^2 + C_B \sigma B h_i + C_V \rho_i v^2 L h_i^{0.65} B^{0.35} \tag{2.4}$$

where C_S, C_B and C_V are empirical values, L is the ship length. The first term of the equation is the submerged resistance, the second term is the breaking resistance and the third term is the velocity dependent resistance. The results from the suggested formulation of Vance (1975) was proven to match close with full-scale measurements from one of the ships.

The equations suggested by Kashteljan et al. (1969), Enkvist (1972) and Vance (1975) are based on empirical values, and in general they are similar as they all consider the same terms such as icebreaking resistance, submerged resistance and speed dependent resistance. However, none of the methods are considering the bow shape, which is remarkable as the bow shape has the largest impact on the icebreaking process and resistance.

2.5.2 Lindqvist (1989)

In the paper of Lindqvist (1989), "A straightforward method for calculation of ice resistance of ships", a formulation for calculating ice resistance based on the following parameters is presented; main dimensions, hull form, ice thickness, friction and ice strength. The method is illustrating how resistance is affected by the given parameters, and the main resistance components defined in the method are crushing and bending due to icebreaking, submersion and speed dependency whereas the speed dependency will increase the resistance significantly in operating speed.

During the breaking process, crushing will occur before bending and the crushing resistance is given by

$$R_c = F_v \frac{\tan\varphi + \frac{\mu\cos\varphi}{\cos\psi}}{1 - \frac{\mu\sin\varphi}{\cos\psi}} \tag{2.5}$$

where F_v is the vertical force acting on the ice from the stem, μ is the friction coefficient, φ is the stem angle and ψ is the angle between the normal of the surface and a vertical vector (the flare angle). The vertical force is given by

$$F_v = 0.5\sigma_b h_i^2 \tag{2.6}$$

where h_i is the ice thickness and σ_b is the bending strength of the ice. The flare angle (the breaking angle) is given as

$$\psi = \arctan(\frac{\tan\varphi}{\sin\alpha}) \tag{2.7}$$

where α is the waterline entrance angle. The bending resistance is expressed as

$$R_b = \frac{27}{64}\sigma_b B \frac{h_i^{1.5}}{\sqrt{\frac{E}{12(1-v^2)g\rho_w}}} \frac{tan\psi + \mu cos\varphi}{cos\psi sin\alpha}(1 + \frac{1}{cos\psi}) \tag{2.8}$$

where B is the breadth of the vessel, E is Young's modulus, v is the Poisson coefficient, ρ_w is the density of the water and g is the gravitational constant. In the breaking process, deflection of the ice and trimming of the vessel are ignored, which is not realistic when applied to ships operating in thick ice conditions.

As the submerged hull is covered in ice when sailing in ice conditions, there is accounted for a submersion component in the total ice resistance due to friction. Assumptions based on this is that the bow is completely covered in ice and also 70% of the submerged hull. The submersion resistance is

$$R_s = \Delta \rho g h_i B \left(\frac{T(B+T)}{B+2T} \right.$$
$$\left. + \mu (0.7L - \frac{T}{\tan \varphi} - \frac{B}{4\tan \alpha} + T\cos \varphi \cos \psi \sqrt{ \left(\frac{1}{\sin \varphi^2} + \frac{1}{\tan \alpha^2} \right) }) \right) \tag{2.9}$$

where $\Delta \rho$ is the density difference between water and ice, T is the draft of the ship and L is the length of the ship. Total ice resistance is then given as

$$R_{ice} = (R_c + R_b)(1 + \frac{1.4v}{\sqrt{gh_i}}) + R_s (1 + \frac{9.4v}{\sqrt{gL}}) \tag{2.10}$$

where v is the ship speed. It can be seen in the formulation that all of the resistance components are assumed to increase linearly with the speed.

The method was validated by using full-scale measurements from seven icebreaking ships in Baltic conditions whereas three of the ships were icebreakers with mainly different main dimensions, while the last four ships had different hull shape. The displacement of the ships were in the range of 70 tons to 13000 tons. The formula was proven to be reliable for larger ships when compared to the real measurements, and the method proves that different hull shapes affects the ice resistance significantly (Lindqvist, 1989). However, as the tests were run in similar ice conditions, the method may have some uncertainties related to estimation of ice resistance in different ice conditions. This means that measurements performed for example in the Arctic region might give different results compared to the measurements done in the Baltic conditions. and therefore it is difficult to conclude the reliability of the method with regard to the ice conditions.

2.5.3 Keinonen et al. (1991, 1996)

The total resistance of an advancing icebreaker in level ice is given by Keinonen et al. (1991, 1996)

$$R_{tot} = R_{ow} + R_{ice,V=1m/s} + R_{ice,V>1m/s} \tag{2.11}$$

where R_{ow} is the open water resistance, $R_{ice,V=1m/s}$ is the icebreaking resistance at 1 m/s and $R_{ice,V>1m/s}$ is the icebreaking resistance at a ship speed above 1 m/s. The icebreaking resistance formula for ship speed at 1 m/s in level ice is presented in the paper of Keinonen et al. (1991) and it is including the icebreaking component, and the components for submergence and clearing. The ice resistance is given for chined hull and rounded hull forms. For chined hull forms, the ice resistance is given as

$$
\begin{aligned}
R_{ice,V=1m/s} = {}& 0.08 + 0.17 \cdot C_s \cdot C_H \\
& \cdot B^{0.7} \cdot L^{0.2} \cdot T^{0.1} \cdot (h_i + 0.5 \cdot H_s)^{1.25} \\
& \cdot (1 - 0.0083 \cdot (t + 30)) \\
& \cdot (0.63 + 0.00074 \cdot \sigma_f) \\
& \cdot (1 + 0.0018 \cdot (90 - \gamma)^{1.4}) \cdot (1 + 0.004 \cdot (\beta_{avg} - 5)^{1.5})
\end{aligned}
\tag{2.12}
$$

where C_H is hull condition factor (describes the roughness of the hull meaning that $C_H = 1$ indicates a frictionless hull), C_s is salinity coefficient, B is ship beam, L is ship length at waterline, T is the draft, h_i is ice thickness, H_s is snow thickness t is surface temperature of ice or air temperature, σ_f is the flexural strength of ice, γ is average bow flare angle in bow region, and β_{avg} is average buttock angle in bow region (Keinonen et al., 1991). For rounded hull forms the ice resistance is

$$
\begin{aligned}
R_{ice,V=1m/s} = {}& 0.015 \cdot C_s \cdot C_H \\
& \cdot B^{0.7} \cdot L^{0.2} \cdot T^{0.1} \cdot (h_i + 0.5 \cdot H_s)^{1.5} \\
& \cdot (1 - 0.0083 \cdot (t + 30)) \\
& \cdot (0.63 + 0.00074 \cdot \sigma_f) \\
& \cdot (1 + 0.0018 \cdot (90 - \gamma)^{1.6}) \cdot (1 + 0.003 \cdot (\beta_{avg} - 5)^{1.5})
\end{aligned}
\tag{2.13}
$$

The term, $(B^{0.7} \cdot L^{0.2} \cdot T^{0.1})$, is the ship size term, the friction term is expressed as $(1 - 0.0083 \cdot (t + 30))$, the ice strength term is expressed by $(0.63 + 0.00074 \cdot \sigma_f)$, and the last term, $(1 + 0.0018 \cdot (90 - \gamma)^{1.6}) \cdot (1 + 0.003(\beta_{avg} - 5)^{1.5})$, is the bow form term. The ice resistance formulation is only valid for a speed of 1 m/s. Keinonen et al. (1996) modified the method to include the speed dependency, and the additional ice resistance for chined hull icbreakers is given as

$$
\begin{aligned}
R_{ice,V>1m/s} = {}& 0.009 \cdot (\frac{v - 1}{\sqrt{gL}}) \cdot C_H \\
& \cdot B^{1.5} \cdot T^{0.5} \cdot h_i \\
& \cdot (1 - 0.0083(t + 30)) \\
& \cdot (1 + 0.0018 \cdot (90 - \gamma)^{1.4}) \cdot (1 + 0.004(\beta_{avg} - 5)^{1.5})
\end{aligned}
\tag{2.14}
$$

where v is ship speed and g is the gravitational acceleration constant. Here as well, the second term is describing the ship size, the third term is the friction term, and the fourth term is the bow form. In this expression, the strength term is excluded. The ice resistance for rounded hull formed vessels with a speed above 1 m/s is expressed as

$$R_{ice,V>1m/s} = 0.009 \cdot (\frac{v-1}{\sqrt{gL}}) \cdot C_H$$
$$\cdot B^{1.5} \cdot T^{0.5} \cdot h_i$$
$$\cdot (1 - 0.0083(t + 30))$$
$$\cdot (1 + 0.0018 \cdot (90 - \gamma)^{1.6}) \cdot (1 + 0.003(\beta_{avg} - 5)^{1.5}) \tag{2.15}$$

The presented formulations for ice resistance at 1 m/s (see Equation 2.12 and 2.13), including the formulation for the open water resistance which is not presented here, are established for rounded hull shape and chined hull shape icebreakers based on full-scale icebreaking trails data of 18 icebreakers and icebreaking vessels with up to 40 000 tonnes in displacement according to Keinonen et al. (1989, 1991). The data was collected from seven vessels operating in the Beaufort Sea and 11 traditional icebreakers. Keinonen et al. (1996) based the modified mathematical models (see Equation 2.14 and 2.15) on full-scale data from five additional vessels, including four traditionally propeller vessels of different size and shape and a multi-purpose icebreaker with azimuth thrusters. The icebreaking trials were performed at different locations and times of the year, such as the Beaufort Sea and the Northern Baltic, and thus the environmental data were different for each trial.

2.5.4   Riska et al. (1997)

The general ice resistance formulation presented by Riska et al. (1997) in "Performance of merchant vessels in ice in the Baltic" is based on level ice and the total resistance R_T is defined as

$$R_T = R_{ow} + R_i \tag{2.16}$$

where R_{ow} is the resistance in open water and R_i is the ice resistance. The method was validated against full-scale data retrieved from ten ice-capable merchant vessels navigating in the Northern Baltic from 1990 to 1994. The collected data was retrieved from ships with displacement about 5500 tons up to around 57000 tons and with different bow shapes, where the waterline entrance angle was ranging from 19 to 40 degrees, and the stem angle from 29 to 68 degrees.

The formulation presented in the paper is based on the formulations derived by Ionov (1988), Lindqvist (1989) and Kämäräinen (1993). The ice resistance formula depends on ice thickness, ship speed, main dimensions and bow shape, and it is only considering level ice. The ice thickness will vary, while the ice strength, ice density, water density and hull/ice friction are seen as constant, and the difference between the water and the ice density is assumed to be 125 kg/m^3, the ice bending strength is 500 kPa, and the friction coefficient is 0.15. The ice resistance is given as

$$R_i = C_1 + C_2 v \tag{2.17}$$

where C_1 and C_2 are constants that are determined by modifying the ice resistance formulation by Ionov (1988) and Lindqvist (1989), and the v is the speed of the ship. The speed dependency is assumed to be linear and the waterline entrance angle, α, is neglected. C_1 and C_2 are given by

$$C_1 = f_1 \frac{1}{2\frac{T}{B}+1} BL_{par}h_i + (1+0.021\varphi)(f_2 Bh_i^2 + f_3 L_{bow}h_i^2 + f_4 BL_{bow}h_i) \tag{2.18}$$

$$C_2 = (1+0.063\varphi)(g_1 h_i^{1.5} + g_2 Bh_i) + g_3 h_i(1 + 1.2\frac{T}{B})\frac{B^2}{\sqrt{L}} \tag{2.19}$$

where the constants f_1, f_2, f_3, f_4, g_1, g_2 and g_3 are given in Table 2.1. The values of the constants are based on the performance of ten actual ships as mentioned earlier. T is the ship draught, B is the breadth, L_{par} is the length of the parallel midbody of the ship at the waterline, h_i is the ice thickness, φ is the stem angle, L_{bow} is the length of bow part of the ship at the waterline and L is the length of the ship.

Table 2.1: The constants used in the equation for ice resistance (Riska et al., 1997).

$f_1 = 0.23 kN/m^3$	$g_1 = 18.9 kN/(m/s * m^{1.5})$
$f_2 = 4.58 kN/m^3$	$g_2 = 0.67 kN/(m/s * m^{1.5})$
$f_3 = 1.47 kN/m^3$	$g_3 = 1.55 kN/(m/s * m^{1.5})$
$f_4 = 0.29 kN/m^3$	

In reality the ice-cover is consisting of both level-ice and ridges, and the paper is suggesting additional formulations for calculating resistance due to ridges and brash ice, but the ridges and the brash ice are not taken into account as a design criteria and will therefore not be further discussed. However, as the features of ridges and brash ice are not included in the presented ice resistance formulation, there will be uncertainties related to ships sailing in other ice conditions than level ice. In addition, the parameters describing the ice strength, the ice density and the friction between hull and ice are seen as constant in this method, which in reality will change due to non-uniform ice properties. However, the paper justifies for the constant values as the measurements are taken from ships operating only in Baltic conditions, and thereby the parameters can be approximated to be constant.

2.6   Comparison and Discussion of the Semi-Empirical Methods

The presented ice resistance methods are considering different parameters and a comparison of the included parameters in each method is shown in Table 2.2. As seen in Table 2.2, the methods from earlier decades Kashteljan et al. (1969), Enkvist (1972) and Vance (1975), are not considering parameters describing the bow shape, which makes the methods insensitive to changes of the bow shape. The three methods are only considering the main dimensions of the vessel, the speed and the ice parameters. If these formulations are applied to calculate

the ice resistance on ships with different bow shape and same main dimensions, the results will be similar, but might be more inaccurate compared to the methods developed in the later years. Thus, the methods can be seen as less reliable as the bow shape affects the ice resistance and icebreaking process significantly.

Table 2.2: Parameters included in the presented ice resistance prediction methods.

Parameter	Symbol	Kashteljan et al. (1968)	Enkvist (1972)	Vance (1975)	Lindqvist (1989)	Keinonen et al. (1991)	Keinonen et al. (1996)	Riska et al. (1997)
Ship beam	B	x	x	x	x	x	x	x
Ship length	L			x	x	x	x	x
Bow length	L_{bow}							x
Length of parallel midbody	L_{par}							x
Ship draught	T		x		x	x	x	x
Waterline entrance angle	α				x			
Average buttock angle in bow region	β_{avg}					x	x	
Stem angle	φ				x			x
Flare angle	ψ				x	x	x	
Average flare angle in bow region	γ					x	x	
Friction coefficient	μ				x			
Hull condition factor	C_H					x	x	
Salinity coefficient	C_S					x	x	
Ice strength	σ	x	x	x	x	x	x	
Ice thickness	H_{ice}	x	x	x	x	x	x	x
Snow thickness	H_s					x		
Gravitational acceleration constant	g		x	x	x		x	x
Elastic modulus of ice	E				x			
Poisson coefficient	ν				x			
Water density	ρ_w		x	x	x			
Ice density	ρ_i	x	x	x	x			
Ship speed	v	x	x	x	x		x	x

From Table 2.2 it can be seen that Lindqvist, Keinonen et al. and Riska et al. are all considering the main dimensions of a ship, but the method that stands out is Riska et al. which considers less parameters than the other two methods and it considers only one bow angle, the stem angle. This is of significance as the bow angles has a big influence on the computed ice resistance.

As the methods of Kashteljan et al. (1969), Enkvist (1972) and Vance (1975) are including certain empirical values, the methods presented by Lindqvist (1989), Keinonen et al. (1991, 1996) and Riska et al. (1997) are compared by computing the ice resistance of two different ships, the coast guard icebreaker KV Svalbard, as presented in Lubbad and Løset (2011), and the ice-going tanker Sotka, as presented in Riska et al. (1997). The input data for the methods can be seen in Table 2.3, where 2.3a represents the ship data and 2.3b contains additional input parameters in the applied methods.

Table 2.3: Input data for the semi-empirical methods.

<table>
<tr><td colspan="3">(a) Ship parameters.</td><td colspan="2">(b) Additional parameters.</td></tr>
<tr><td>Parameter</td><td>KV Svalbard</td><td>Sotka</td><td>Parameter</td><td>Value</td></tr>
<tr><td>L_{pp} [m]</td><td>89</td><td>150</td><td>h_i [m]</td><td>0.45, 0.95</td></tr>
<tr><td>B [m]</td><td>19.1</td><td>21.5</td><td>σ_b [kPa]</td><td>550</td></tr>
<tr><td>T [m]</td><td>6.5</td><td>9.5</td><td>ρ_i [tonnes/m^3]</td><td>0.900</td></tr>
<tr><td>L_{bow} [m]</td><td>27.2</td><td>32.4</td><td>ρ_w [tonnes/m^3]</td><td>1.025</td></tr>
<tr><td>L_{par} [m]</td><td>36.32</td><td>77</td><td>g [m/s^2]</td><td>9.81</td></tr>
<tr><td>α [degrees]</td><td>59</td><td>24</td><td>E [kPa]</td><td>$2 \cdot 10^6$</td></tr>
<tr><td>φ [degrees]</td><td>33</td><td>29</td><td>μ [-]</td><td>0.1</td></tr>
<tr><td>ϕ_{avg} [degrees]</td><td>30</td><td>29</td><td>υ [-]</td><td>0.3</td></tr>
<tr><td></td><td></td><td></td><td>H_s [m]</td><td>0</td></tr>
<tr><td></td><td></td><td></td><td>C_H [-]</td><td>1.15</td></tr>
<tr><td></td><td></td><td></td><td>C_s [-]</td><td>0.85</td></tr>
<tr><td></td><td></td><td></td><td>t [Celsius degrees]</td><td>0</td></tr>
</table>

The resulting ice resistance curves by applying each method for h_i =0.45m and h_i = 0.95m can be seen in 2.6 and 2.7. The blue lines represents the results obtained from Lindqvist, the cyanide coloured lines are results from Riska et al., and the red lines indicates the results obtained from Keinonen et al.
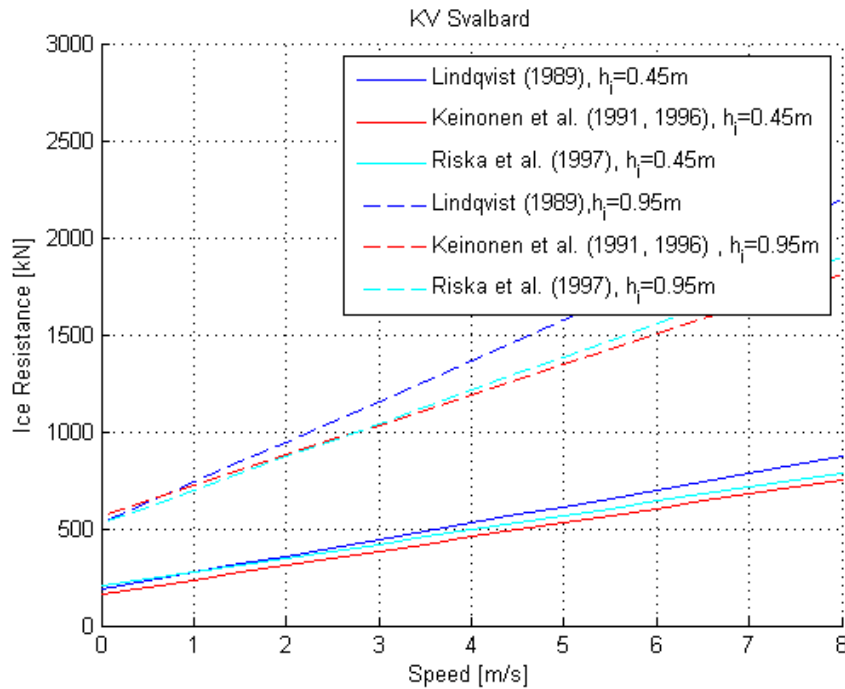
Figure 2.6: Resistance curves for KV Svalbard for h_i=0.45m and h_i=0.95m by applying Lindqvist (1989), Keinonen et al. (1991, 1996) and Riska et al. (1997) .
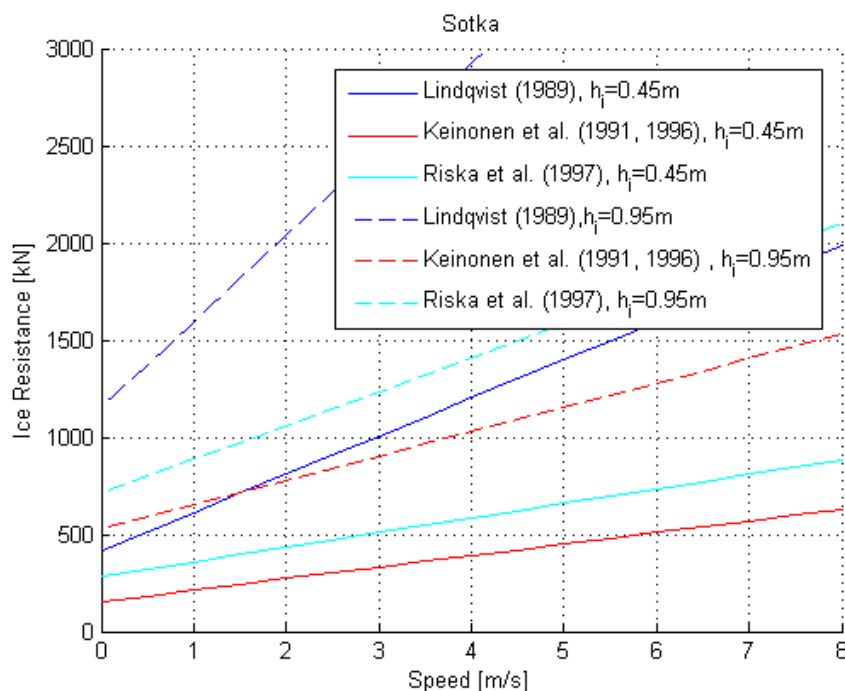
Figure 2.7: Resistance curves for Sotka for h_i=0.45m and h_i=0.95m by applying Lindqvist (1989), Keinonen et al. (1991, 1996) and Riska et al. (1997).

The resulting resistance curves for KV Svalbard in Figure 2.6 indicate that the applied methods are giving similar results for both of the two ice thicknesses. Overall, Lindqvist is giving higher ice resistance for an increasing ship speed, while the resulting curves obtained by Keinonen et al. and Riska et al. are less deviating and will give similar results.

For Sotka, it can be seen in Figure 2.7 that the ice resistance curves are quite deviating. Lindqvist will give a significant higher resistance compared to the other two methods. As the method of Lindqvist is validated against full-scale measurements from ships up to 13000 tons, while Sotka has a displacement of 22033 tons (Riska et al., 1997), this might indicate that the method is not applicable for such large ships. In addition, the method might also be sensitive to a change of the bow shape angles as Sotka has a waterline entrance angle which is around 40% of the waterline entrance angle of KV Svalbard.

2.7 Numerical Methods for Ice Resistance Prediction

As previously mentioned in Section 2.1, the developed icebreaking pattern caused by the ship-ice interaction can influence the magnitude of ice forces acting on the ship hull. Several numerical models have been developed through the last decade and the focus has been set towards the physics of the icebreaking process as knowledge about the process can increase the reliability of the methods. The methods emphasize the ship-ice interaction, how the ice cover will fail and thus the predefinition of the ice cusp shape, which are broken off the level ice edge due to formation of cracks in the ice.

The shape of the ice cusps was assumed to be semi-elliptical according to Naegle (1980) due to observations from full-scale ice trials. Lindstrom (1990) developed a method for computing the dynamic loads and average ice forces on sloping structures and ships in uniform ice thickness, and the defined ice cusp geometry by Naegle (1980) was used to calculate ice forces acting on a ship advancing in level ice. The approach of Naegle was later modified by Kotras et al. (1983) in order to include additional ice cusp shapes observed in the ice trails, which was done by adding wedge-shaped ice pieces between semi-elliptical ice cusps (Kotras et al., 1983). Wang (2001) presented a model which simulated the interaction between the ice cover and conical structures where the bending of ice in the icebreaking process was predefined after the bending model of Milano (1973). In addition, Wang (2001) developed a formula estimating the broken ice cusp radius, which has later been used in several methods.

Some of the numerical methods for ice resistance prediction developed in the last decade will be presented and discussed, which are the methods of Valanto (2001), Liu et al. (2006), Sawamura et al. (2009), Lubbad and Løset (2011), Su et al. (2010) and Erceg et al. (2014).

2.7.1 Valanto (2001)

Valanto (2001) developed a 3D numerical model of the icebreaking process on the waterline of a ship in level ice. The model was applied to calculate resistance forces and ice loads on ship hull in addition to evaluate the underwater components by applying the semi-empirical method of Lindqvist (1989). The method of Lindqvist (1989) was applied as the modeling of the processes on the underwater hull causing resistance was not complete. The total resistance in level ice is thus the sum of these components. Valanto (2001) is considering crushing at stem and bending of ice as a part of the breaking components of ice resistance. In addition, the rotation of the ice floes is considered, whereas ventilation is included which will cause an additional resistance force.

The numerical method of Valanto is including a simulation of the response of the floating level ice cover and the surrounding fluid to the navigating ship. The model is describing the behavior of the floating ice cover before and after flexural failure in the ice. The icebreaking process involves ice cusps breaking from the ice cover, which happens with a certain randomness. The breaking of the ice cusps is influenced by the hull shape angles, ship speed, ice properties and the flow field induced by the motion of the ship. The ice cusp processes were assumed to be independent from each other, which means no interaction. Due to this assumption, the ice resistance on the hull is computed by dividing the icebreaking part of the waterline into separate segments where the ice resistance forces were calculated for each segment and summed up to obtain the total ice breaking force.

2.7.2 Liu et al. (2006)

Liu et al. (2006) developed an ice-hull interaction model where the icebreaking process is numerically simulated in the time domain. The background for the development of this model was that no earlier models, such as the models of Lindstrom (1990) and Valanto (2001), could satisfy the requirements of the Centre for Marine Simulations' simulator, which required simulations of arbitrary ship manoeuvres in ice. The developed model follows a preliminary model presented by Lau and Derradji-Aouat (2004).

The total force is found by summing the following three force components: breaking, buoy-ancy and clearing forces, which all occur during the icebreaking process. The contact area in the ship hull-ice interaction is calculated based on a time domain methodology. The methodology involves that the contact area between the hull and the ice is estimated at the next step based on the current channel and the ship motion. When the contact area is esti-mated, the ice breaking force can be found. An illustration of the hull-ice interaction in the framework is seen in Figure 2.8.
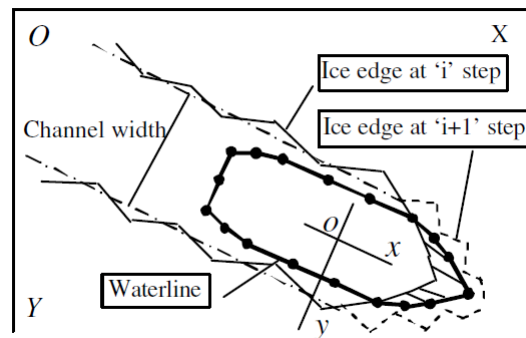
Figure 2.8: Interaction between ship hull and ice given in the time domain methodology (Liu et al., 2006).

The icebreaking pattern in the model is illustrated in Figure 2.9 after Kotras et al. (1983), whereas D is describing the average breaking depth, and W is the width of the ice cusps, which is based on the full-scale trials of Kotras et al. (1983).
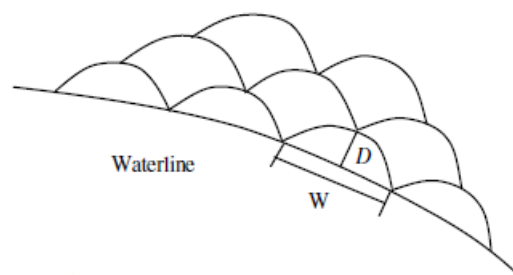
Figure 2.9: Ice cusp pattern (Liu et al., 2006).

In this method, the ship hull is divided into segments and the breaking force and the clearing force is calculated at each hull segment separately, and in the end, the two force components on each segment are summed up. The bottom of the ship is assumed to be flat for the buoy-ancy force calculations and all of the force components are summed up to find the total ice force on the hull. To calculate the force components, three angles describing the bow shape are included: the waterline entrance angle, the stem angle and the flare angle. In addition, the method is considering ice properties such as ice thickness, density and strength, and also ship velocity (Liu et al., 2006).

2.7.3   Sawamura et al. (2009)

The paper of Sawamura et al. (2009) is presenting a numerical method for calculating the icebreaking pattern and ice load for a ship advancing in level ice, which follows the method of Wang (2001). As Valanto (2001) developed a 3D numerical model which is considering relatively simple ice edge in the ship-ice interaction, Sawamura is considering the dynamic response of floating ice with various kinds of the ice edge by applying the Finite Element simulation carried out by Sawamura et al. (2008).

During the ship-ice interaction, there will occur contact points between the ship and the level ice edge. The forces acting on the ship hull will be calculated in the detected contact points and the contact points are determined by using the circle contact detection technique, which is illustrated in Figure 2.10. The ship-ice interaction region will be covered by circles and the broken-off ice floes will be assumed to have a circular shape. A smaller circle radius will give a more accurate contact detection, and the results in the paper of Sawamura et al. (2009) proves that the icebreaking pattern is influenced by the radius of the ice circles (Wang, 2001).
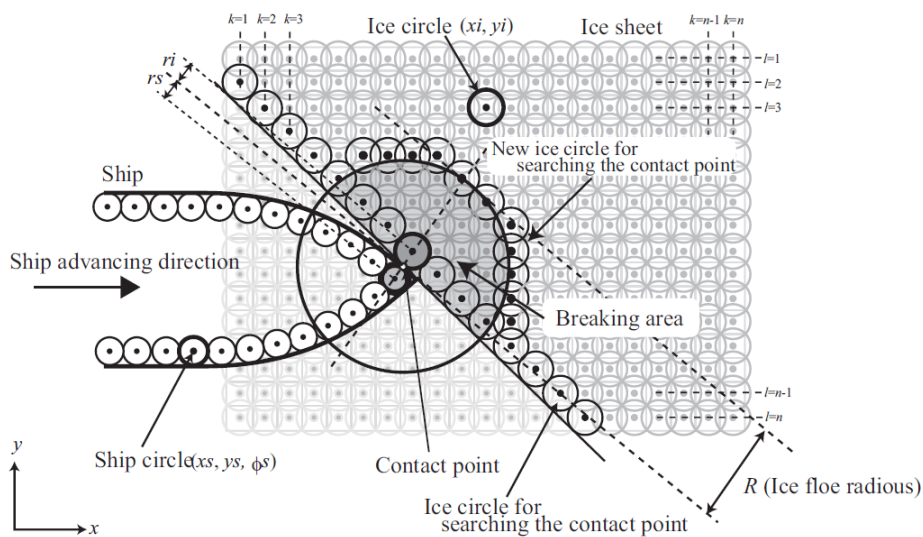
Figure 2.10: Circle contact detection technique (Sawamura et al., 2009).

The method is considering parameters such as contact angle of ship, θ_c, ship hull angle at contact plane, θ_s, ship velocity, v, ice thickness, h_i, an dynamic friction coefficient, μ (Sawamura et al., 2009).

2.7.4   Lubbad and Løset (2011)

Lubbad and Løset (2011) presents a numerical model which simulates the ship-ice interaction process in real-time. The method consists mainly of a Mathematical Ship Model (MSM) and Mathematical Ice Model (MIM) connected by a feedback loop, where the MSM computes the ship position and the MIM computes the ice forces. The results obtained from the simulations are validated against model tests data and full-scale measurements.

To calculate the ice forces, two modules are used; rigid body motion module and ice break-ing module. The rigid body motion module will calculate the response of the unbreakable ice floes and estimates their actions on the ship hull by solving the rigid body equations for motion. The ice breaking module calculates the response of the breakable ice floes and esti-mates their action on the ship hull. The contact model in the ice breaking module includes calculation of the contact area where the contact area is estimated by surrounding the sur-face of ice floe and the ship hull by 2D polygons. This is illustrated in Figure 2.11. The points of the intersection between ship and ice polygons, and the vertices of ship and ice polygons entering each others polygons are located to define the intersection polygon. When the in-tersection polygon is defined, the contact area between and ship and ice can be estimated.
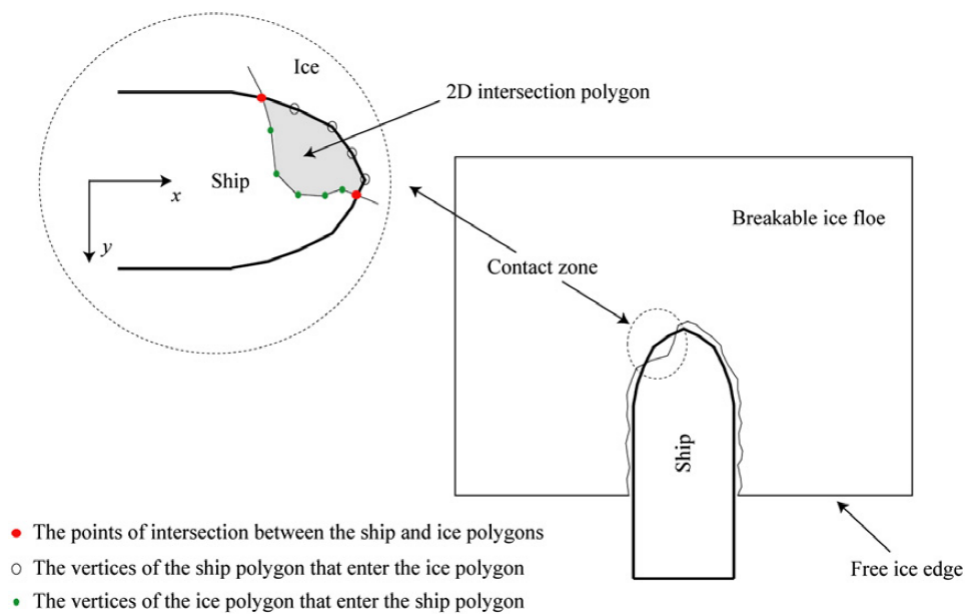
Figure 2.11: Ship hull-ice intersection area (Lubbad and Løset, 2011).

The stresses in the ice floe caused by the hull-ice interaction are evaluated using the theory of a semi-infinite plate resting on an elastic foundation, and if the stresses reach the failure criterion for the ice floe, wedges will be created and thus the generated cusps are consid-ered as wedge-shaped. The failure criteria are defined as semi-infinite plate failure (which includes formation of radial cracks), and wedge-shaped beam failure, (which is formation of circumferential cracks). The first radial crack is initiated at the free ice edge when the bend-ing stress in the plate has reached the flexural ice strength. More radial cracks will formed and the model of the semi-infinite plate resting on elastic foundation will now be replaced with the adjacent wedge-shaped beams resting on elastic foundation (Nevel, 1958, 1961). Circumferential cracks will be generated when the maximum bending stress in the wedge-shaped beams exceed the flexural strength of ice and thus the ice cusps will be broken off. An illustration of the replacement of the semi-infinite plate model with the adjacent wedge-shaped beams model resting on an elastic formation can be seen in Figure 2.12 (Lubbad and Løset, 2011).
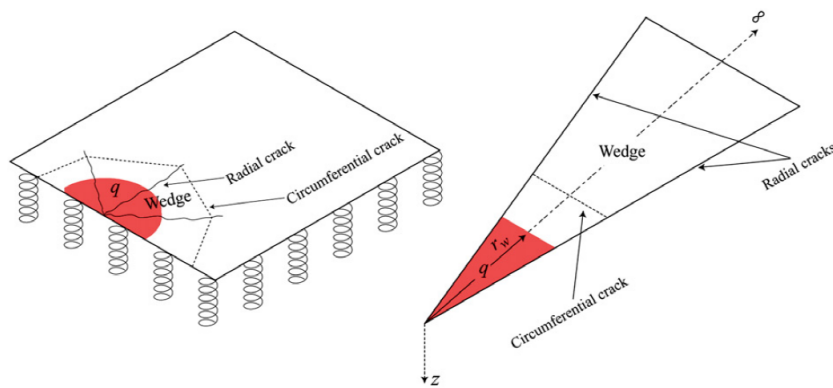
Figure 2.12: The semi-infinite plate model replaced by the model of adjacent wedge-shaped beams resting on an elastic foundation (Lubbad and Løset, 2011).

2.7.5   Su et al. (2010)

Su et al. (2010) developed a numerical model in order to simulate the ice-hull interaction and ship maneuvres in level ice, where the ship performance in level ice and the ice loads on the ship hull are estimated. The model is partly based on empirical data and it was validated against full-scale measurements from the icebreaker Tor Viking II. The icebreaking process in this method follows the ice failure model of Wang (2001) which is based on an empirical equation introduced by Kashtelyan in Kerr (1975) (Su et al., 2010).

The breaking process of ice in the model of Su is divided in two main components; an ice-breaking component and an ice displacement component. The icebreaking component is including crushing at the stem, shoulder crushing and bending of ice, which are all found numerically. The ice displacement component in the model is based on Lindqvist (1989), which includes turning, submerging and sliding of ice floes.

In order to calculate the icebreaking component, the contact area between the ship hull and ice has to be found. The hull and the ice are discretized into a closed polygon and a polyline, respectively. The simulation program will collect the nodes on the ice edge which are inside the hull polygon on each step by using computer geometric tools, and thus the contact area can be found. The discretization and the hull-ice interaction are illustrated in Figure 2.13, and the contact area is illustrated in Figure 2.14a where L_h is representing the contact length, L_d is the indentation depth in the contact zone, and φ is the slope angle of the ship hull (Su et al., 2010).
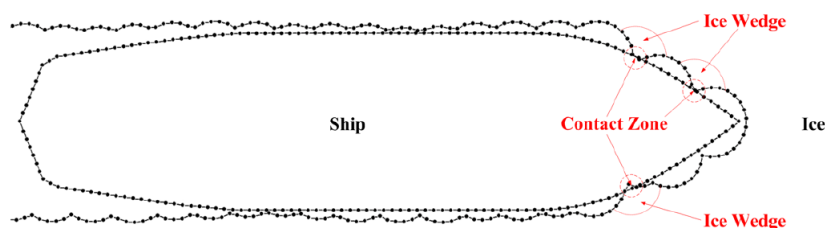
Figure 2.13: Ship hull-ice interaction (Su et al., 2010).

The ice wedges that are broken of the ice sheet are idealized as an arc and an illustration of an idealized ice wedge can be seen in Figure 2.14b. The size and the curvature of the ice cusp is determined by the interpolation of breaking radius, which is found by an expression given by Wang (2001), and the size of the ice cusp is depending on speed, characteristic ice length and frame angle (Tan et al., 2013).
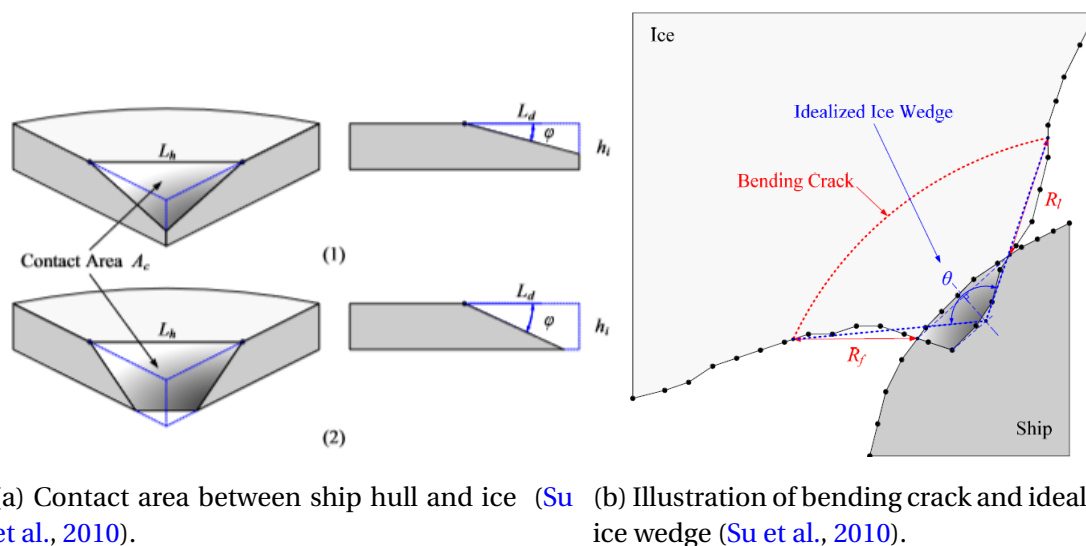
(a) Contact area between ship hull and ice (Su et al., 2010).

(b) Illustration of bending crack and idealized ice wedge (Su et al., 2010).

Figure 2.14: Contact zone and idealized ice wedge.

2.7.6 Erceg et al. (2014)

In the paper of Erceg et al. (2014), a quasi-static numerical method was developed in order to model the initiation of the icebreaking pattern of a ship advancing in level ice. The initiation process indicates the creation of circumferential ice cracks, while ignoring the following radial cracks. The method considers the bow geometry and the properties of the encountered ice. The bow geometry includes the waterline entrance angle, α, the buttock angle, ϕ, and the flare angle, ψ, and the ice properties are described by the ice thickness, h, flexural strength, σ_f, elastic modulus, E, and friction coefficient, μ. An illustration of the concept used in the model is seen in Figure 2.15.

The concept in the model is based on radially oriented ice beams in the contact zone between the ship and the level ice sheet, which are oriented by the angle β. The radial ice beams will discretize the level ice sheet to obtain irregular shapes of ice cusps (Erceg et al., 2014). Figure 2.16 illustrates the ice cusp creation whereas the ice cusp will continue to propagate at d_n, which is the outermost failure point to the nearest ice edge, with an angle γ.

The model of Erceg et al. (2014) is not accounting for the ship motions and thus the effects of irregularity and non-uniformity due to simulation of icebreaking patterns will be disregarded.
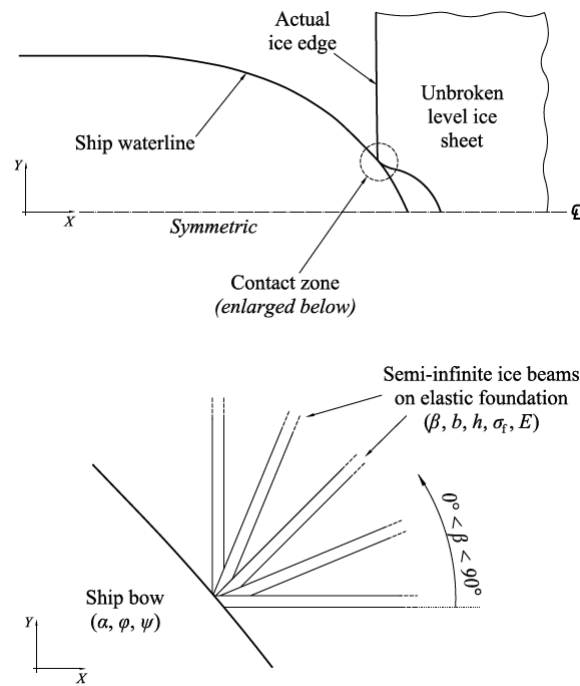
Figure 2.15: Ship-ice interaction (top) and the conecept of radial ice beams (bottom) (Erceg et al., 2014).
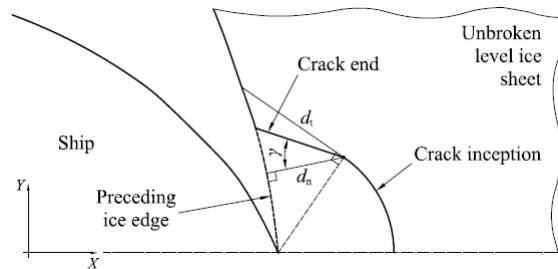
Figure 2.16: Creation of ice cusp according to the model (Erceg et al., 2014).

2.7.7   Comparison and Discussion of the Numerical Methods

The presented numerical methods are considering several common parameters for ice resistance prediction, and the ship parameters having largest impact on ice resistance can be seen as the bow shape angles. The significant difference between the methods is the predefinition of the ice cusp geometry. Many of the presented methods are defining the shape of the ice cusps as specific, such as elliptical, circular or wedge-shaped, which are based on observations from model- and full-scale tests. Erceg et al. (2014) have developed a method which can provide a prediction of irregular ice cusp shapes, which will results in a more realistic ice-breaking pattern compared with the other numerical methods as in reality the icebreaking pattern does not consist of regular ice cusp shapes due to non-homogeneous properties.

The semi-empirical methods discussed in Section 2.5 are not considering the physical effects

of the icebreaking process, and thus not the created icebreaking pattern either. By applying numerical methods, the ice resistance can be estimated by considering the icebreaking process with regard to the ice cusp geometry, which might give more accurate results compared to results obtained by applying semi-empirical methods. However, numerical ice resistance prediction methods are quite complex and time consuming and in some cases it might be preferable to use a semi-empirical approach to save time and to limit the complexity. This will be further discussed in Section 2.8.

2.8 Comparison of a Semi-Empirical and a Numerical Method

In this chapter one semi-empirical method and one numerical method will be compared to identify the deviation between the different type of methods. The chosen semi-empirical method is Lindqvist (1989) as this method is applied in several numerical methods to calculate ice forces, and the method of Su et al. (2010) is chosen to be the investigated numerical method. The deviation will justify whether one of the methods are more preferable to use or not.

In order to compare the methods, both of the methods have to be applied. However, the numerical method is complicated and it is difficult to obtain any results without performing simulation. Due to this, the results from Su's method are retrieved from Su's doctoral thesis "Numerical Prediction of Global and Local Ice Loads on Ships" (2011). Su (2011) did investigate the level ice performance of the Swedish multi-purpose icebreaker Tor Viking II by comparing simulation results with field measurements. The ship parameters from Tor Viking II will thus be used in the method of Lindqvist (1989) in order to obtain comparable results.

The input data for Lindqvist's method are given in Table 2.4, where the ship data of Tor Viking II Su (2011) can be seen in Table 2.4a and the data of ice properties are given in Table 2.4b. The parameters in Table 2.4 are mainly based on data used in the paper of Lindqvist (1989) and Su (2011), and some of the values are assumed.

Table 2.4: Input data for Linqvist's method.

(a) Data from Tor Viking II.

Parameter	Value
L_{oa} [m]	83.7
L_{pp} [m]	75.2
B [m]	18.0
T [m]	6.5
P_D [kW]	13 440
D_P [m]	4.1
v_{ow} [knots]	16.4
α [degrees]	32
φ [degrees]	26

(b) Ice properties.

Parameter	Value
σ_b [kPa]	550
ρ_i [tonnes/m^3]	0.900
ρ_w [tonnes/m^3]	1.025
g [m/s^2]	9.81
E [N/m^2]	$2 \cdot 10^9$
v [-]	0.3
μ [-]	0.1

To determine the ship performance of Tor Viking II, the curve for ice resistance versus ship speed has to be determined first, which will vary with level ice thicknesses. Furthermore, the net thrust that will overcome the ice resistance has to be calculated, which can be found by applying Equation 2.1. The intersection points between the ice resistance curve at each ice thickness and the net thrust curve, will define the points on the ice thickness versus ship speed curve (ship performance curve). The range of level ice thicknesses used in the calculation is from 0.2 m to 1.2 m.

The resulting ice resistance curves for different ice thicknesses and the net thrust curve can be seen in Figure 2.17. The ship performance curve is generated based on the intersection points in Figure 2.17, and the resulting ship performance curve by applying Lindqvist's method can be seen in Figure 2.18. The comparison of the h-v curves are presented in Figure 2.18, whereas results obtained by Su's simulation and measurements from full-scale trials in Riska et al. (2001) are included.
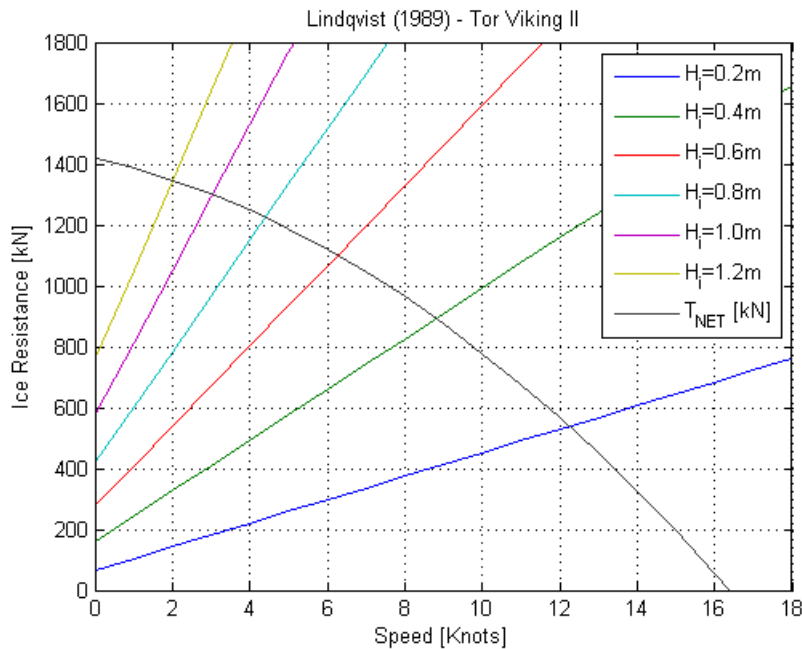
Figure 2.17: Ice resistance curves for specified ice thicknesses and net thrust curve for Tor Viking II.

The results from the paper of Su (2011) in Figure 2.18 are found by a simulation with a free-running model, whereas the motion of the ship is obtained by solving the equations of motion, which is a part of Su's numerical method. The submersion and the friction resistance are found by applying Lindqvist's method and the breaking resistance is found numerically. The results from the full-scale trials are based on effective ice thickness, which means that the snow thickness has been taken into account by increasing the ice thickness by one third of the snow layer thickness (Riska et al., 2001).
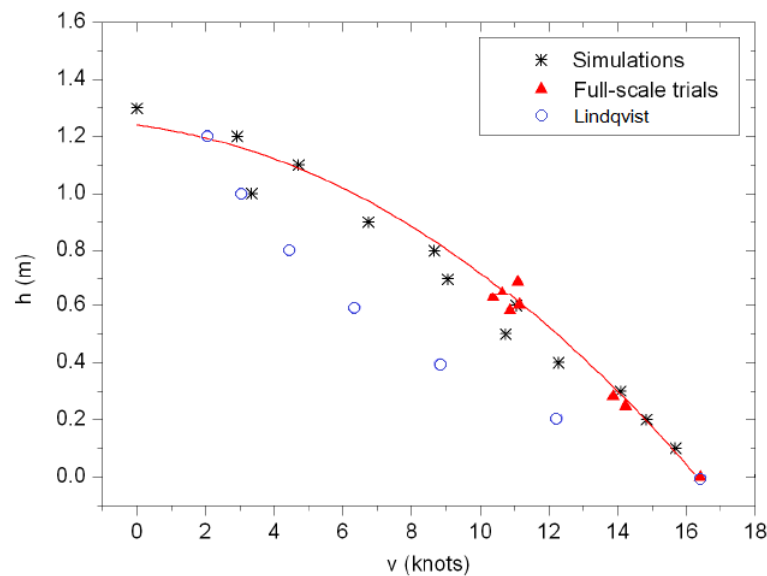
Figure 2.18: Comparison of the ship performance curve between the simulations performed by Su (2011), full-scale measurements presented by Riska et al. (2001) and results obtained by applying the method of Lindqvist (1989).

If the results in Figure 2.18 are compared, it can be seen that the ship performance derived from Lindqvist's formulation is in overall lower than the results obtained by Su's method. The ship motion, nor the general hull shape are considered in Lindqvist's method, which means that shoulder crushing has not been taken into account when applying the formulation. Shoulder crushing will cause increased breaking resistance, which may affect the ship performance in ice significantly.

When estimating the net thrust and the ice resistance of the ship, the formulations have to be applied with caution as certain factors are not considered. The net thrust formulation is not considering propeller and ice interaction (Riska, 2011a) and the ship performance plot is therefore not corrected for the propeller-ice interaction. In addition, Tor Viking II will have a minimum forward speed in order to be able to proceed in level ice due to ice resistance at zero forward speed. The minimum forward speed is unknown and by that not considered in the calculations. In addition, any possible snow layer on top of the ice is neglected in the method of Lindqvist. A snow layer would give increased friction between the ship hull and the ice and therefore increase the resistance. This implies that in theory Lindqvist's method should give lower ship performance due to an increased resistance. As Su's approach is partially including the application of Lindqvist's method, the results obtained by this method are also expected to be somewhat lower. In addition, it must be taken into consideration that in the field measurements of the full-scale trials there will be variation in ice thickness, while in the methods of Su and Lindqvist the ice thickness is seen as constant.

Overall, the results in Figure 2.18 justify the application of the numerical method rather than the semi-empirical method as it gives more accurate results when compared to the full-scale measurements. Furthermore, it should be noted that the results are from only one ship and for given ice conditions. As presented in Section 2.6, where a comparison of the reviewed

semi-empirical methods was performed by using ship data from two ships (see Figure 2.6 and Figure 2.7), Lindqvist's method will give deviating results for different ships with regard to the size and bow shape and thus the results should be considered with caution. In addition, this comparison was performed for one numerical method and one semi-empirical method, and most likely other methods will give deviating results due to underlying assumptions.

3. Description of the Parametric 3D Model

In order to be able to generate desired bow shapes based on bow geometry, and to develop a model which is applicable for ice resistance prediction methods and simple to use, a parametric 3D model was developed by using MATLAB.

Section 3.1 is presenting the "bow skeleton" for the generated bow shape, which is the basis of the 3D bow shape. Section 3.2 is describing the surface added to the bow skeleton, which consists of non-uniform rational basis spline (NURBS) surface, and how the NURBS surface is built up. The last section, 3.3, is presenting a flow chart of how the MATLAB code functions, and the calling functions with the corresponding input and output parameters.

3.1   Bow skeleton

The starting point for the parametric 3D model was to first develop a "bow skeleton" that would describe the bow shape without adding any surface. The bow skeleton is made up by a 4-by-4 mesh grid and the points in the mesh grid are defined as control points which will depend on the dimension of the bow, ice thickness and the bow shape angles. When values for these parameters are inserted, the control points will adjust accordingly and the model will be scaled automatically. After defining the bow skeleton, the surface was added to generate the curves of the bow, which will be further discussed and presented in Section 3.2.

The bow skeleton is illustrated in Figure 3.1, 3.2 and 3.3, where 3.1 is illustrating the top view, 3.2 is the front view and 3.3 is representing the starboard view of the bow skeleton with included control point annotations. The centerline (CL) is located at $y = 0$ running along the x-axis (see Figure 3.1), which means that the longitudinal axis of the ship is along the x-axis. The transverse axis of the ship will run along the y-axis and the draught is described along the z-axis. To obtain a three-dimensional shape, the mesh grid is mirrored about the x-axis.

It can be seen from Figure 3.1, 3.2 and 3.3 that the control points are connected by blue and red lines. The blue lines plotted between control point (2,1), (2,2), (2,3) and (2,4) in Figure 3.3 will be defined as the bottom surface of the level ice sheet, while the blue lines connecting control point (3,1), (3,2), (3,3) and (3,4) will represent the top surface of the ice sheet. For simplicity it is assumed that the ice top surface is corresponding to the waterline of the ship.

31
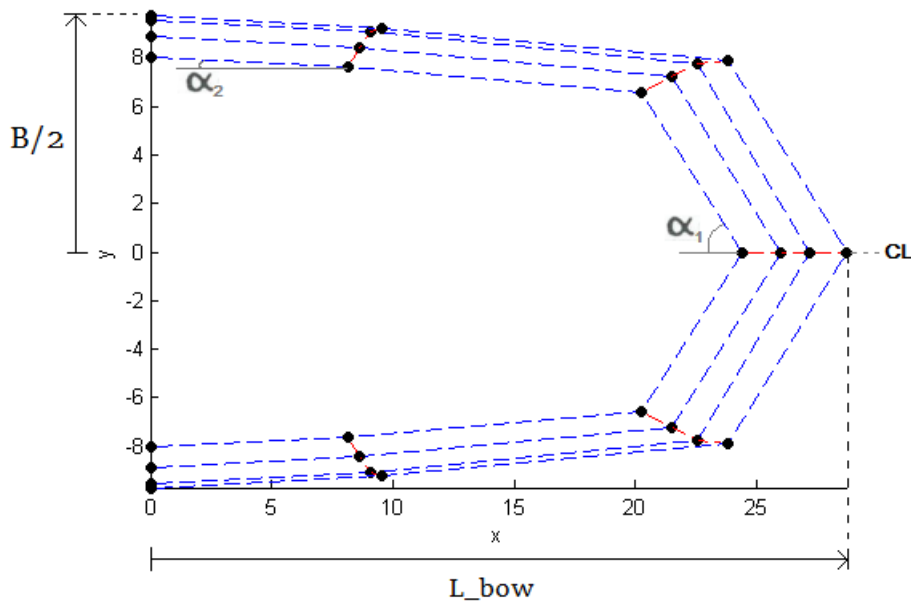
Figure 3.1: Top view of the 3D bow skeleton.
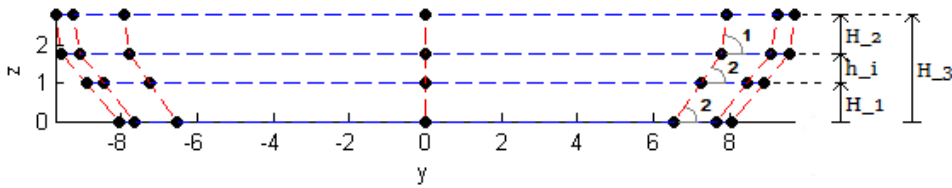
Figure 3.2: Front view of the 3D bow skeleton.
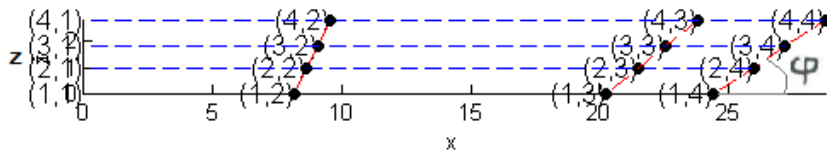
Figure 3.3: Starboard view of 3D bow skeleton with point annotation.

The control points are depending on the following parameters: bow length, L_{bow}, ship beam, B, height from $z = 0$ to the ice bottom surface, H_1 (given as 1 m), ice thickness, h_i, and H_2, which is the height from the waterline to the top of the bow (given as 1 m). The model is only considering the area which interacts with the ice edge, which in this case will be defined by the investigated ice thickness, in addition to a certain height under and above the ice thickness described respectively by H_1 and H_2, which is assumed to be the ice belt. The bottom and top of the bow is excluded to keep the model simple and because the ice resistance prediction methods are only considering the area interacting with the ice edge when

computing the breaking resistance. Furthermore, it is complex to model the bottom of the bow and therefore this part will not be included in the model developed in this thesis.

Further, the model will additionally depend on angles describing the bow shape, such as two waterline entrance angles, α_1 and α_2, two frame angles, β_1 and β_2, and the stem angle, φ. Since the control points are integrated in a mesh grid, the lines in the mesh grid will not be curved. To obtain a shape that can be seen as realistic and to keep the number of parameters low (to attain a simple model), the control points will depend on two waterline entrance angles and two frame angles. If the model depended on one waterline entrance angle and one frame angle, the generated bow shape would look less realistic due to more straight sides and thus the computed bow shape angles will be equal between the control points, which is not desired. In addition, a parameter called $radScale$, with initial value equal to one, will move the control points (1,3), (2,3), (3,3) and (4,3) further away or closer to the stem in x-direction by either increasing or decreasing the value respectively. By increasing $radScale$ with 0.1 to 0.5, a spoon-shaped bow can be obtained for a large α_1. For a small α_1, a wedge-shaped bow will be achieved, but to avoid the stem to be very sharp, $radScale$ can be decreased with 0.1 to 0.5 to obtain a more rounded and realistic stem. If the parameters are changed in the model, the control points will automatically adjust as there are interdependencies between the control points. If for example L_{bow} is changed, the x-coordinates in each control point will change as they are scaled up depending on L_{bow}.

The definition of α_1 and α_2 can be seen in Figure 3.1. α_1 is defined as the angle between the control points (1,3), (2,3), (3,3), (4,3) and (1,4), (2,4), (3,4), (4,4), and α_2 is the angle between the control points (1,1), (2,1), (3,1), (4,1) and (1,2), (2,2), (3,2), (4,2) in the xy-plane. β_1 and β_2 are illustrated as 1 and 2 respectively in Figure 3.2 where β_1 is the angle between the control points (3,1), (3,2), (3,3), (3,4) and (4,1), (4,2), (4,3), (4,4), and β_2 is the angle between the control points (1,1), (1,2), (1,3), (1,4) and (3,1), (3,2), (3,3), (3,4) in the yz-plane. The last angle, φ, is defined in Figure 3.3.

To verify that the developed code in MATLAB would generate a realistic bow shape, the data of KV Svalbard were implemented as input values. The ship parameters for KV Svalbard are given in Table 3.1. Figure 3.1, 3.2 and 3.3 are thus generated based on the values from KV Svalbard and for α_2 = 3 degrees, β_1 = 80 degrees, β_2 = 50 degrees and h_i = 0.8 m. The average value for the waterline entrance angle given in Table 3.1 is used for α_1 in the parametric model. This will be somewhat incorrect as α_1 is not an average value, but this did not matter as the purpose was to test if the model generated a realistic bow shape.

Table 3.1: Data of KV Svalbard found in Lubbad and Løset (2011).

Parameter	Value	Unit
L_{pp}	89	m
B	19.1	m
T	6.5	m
L_{bow}	27.2	m
α_{avg}	59	degrees
φ	33	degrees
ϕ_{avg}	30	degrees
ψ_{avg}	32	degrees

3.2   Non-Uniform Rational Basis Spline (NURBS) Surface

In order to apply a surface onto the bow skeleton in obtain a three-dimensional bow shape, NURBS are used to create the surface. NURBS surface is built up on basis spline (B-spline) functions, which will generate a three-dimensional surface. B-spline surface is a polynomial surface, and NURBS surface is thus defined as a non-uniform rational B-spline surface (Schneider and Eberly, 2002). B-spline surface is consisting of control points, knots and knot vectors, where the knot vector is a set of parameters determining how and where the control points will affect the NURBS surface (Meng and Jin, 2011). To create a NURBS surface, which consists of planar patches, two-dimensional grid made of splines and control points is applied. The patches are then parametrized with two variables called s and t where s is a parameter array of row-direction knots and t is parameter array of column-direction knots.

The knots in a B-spline surface are described as $\{s_i\}_{i=0}^{n_0}$ and as $\{t_i\}_{i=0}^{n_i}$, where $s_i \leq s_{i+1}$ and $t_i \leq t_{i+1}$ for all i. A B-spline rectangle patch is desired by the control points P_{i_0, i_1} for $0 \leq i_0 \leq n_0$ and $0 \leq i_1 \leq n_1$, which can be seen in Appendix A, Equation A.1 together with the polynomials $B_{i,0}^{(0)}(s)$, $B_{i,j}^{(0)}(s)$, $B_{i,0}^{(1)}(t)$ and $B_{i,j}^{(1)}(t)$ given by Equation A.2, A.3, A.4 and A.5 respectively (Schneider and Eberly, 2002).

According to Schneider and Eberly (2002), a NURBS surface is obtained from a non-uniform B-spline polynomial surface in three dimensions, which is described as

$$(Y(s,t), w(s,t)) = \sum_{i_0=0}^{n_0} \sum_{i_1=0}^{n_1} B_{i_0,j_0}^{(0)}(s) B_{i_1,j_1}^{(1)}(t) w_{i_0,i_1}(P_{i_0,i_1}, 1) \tag{3.1}$$

where $B_{i_0,j_0}^{(0)}(s)$ and $B_{i_1,j_1}^{(1)}(t)$ are the polynomials described in Equation A.3 and A.5 respectively, and $(P_{i_0,i_1}, 1)$ are control points for $0 \leq i_0 \leq n_0$ and $0 \leq i_1 \leq n_1$ with weights $w_{i_0,i_1} > 0$. When the weights of the control points are the same, the curve is rational. The NURBS surface is obtained based on a polynomial surface by applying the following Equations and obtaining a projection in three dimensions

$$X(s,t) = \frac{Y(s,t)}{w(s,t,)} = \sum_{i_0=0}^{n_0} \sum_{i_1=0}^{n_1} R_{i_0,i_1,j_0,j_1}(s,t) P_{i_0,i_1} \tag{3.2}$$

where

$$R_{i_0,i_1,j_0,j_1}(s,t) = \frac{w_{i_0,i_1} B_{i_0,j_0}^{(0)}(s) B_{i_1,j_1}^{(1)}(t)}{\sum\limits_{k_0=0}^{n_0} \sum\limits_{k_1=0}^{n_1} w_{k_0,k_1} B_{k_0,j_0}^{(0)}(s) B_{k_1,j_1}^{(1)}(t)} \tag{3.3}$$

The B-spline function is already integrated in MATLAB as the function "spcol" which will generate a B-spline collocation matrix. The Equations 3.2 and 3.3 for a NURBS surface were implemented into MATLAB to create a NURBS surface onto the bow skeleton presented in Section 3.1. The resulting bow shape can be seen in Figure 3.4 - 3.7, where Figure 3.4 is illustrating a 3D view of the bow, Figure 3.5 is illustrating the top view, Figure 3.6 is the front view and Figure 3.7 is presenting the port side view.
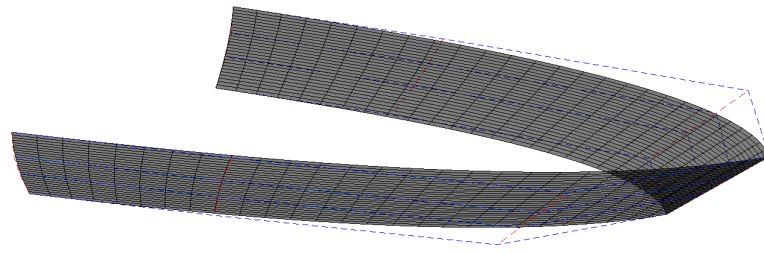
Figure 3.4: 3D bow shape.
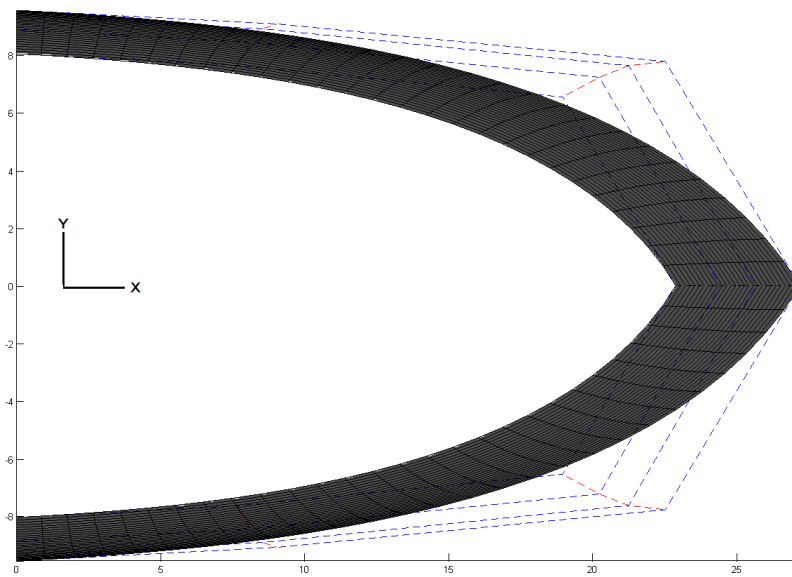
Figure 3.5: Top view of the 3D bow shape.
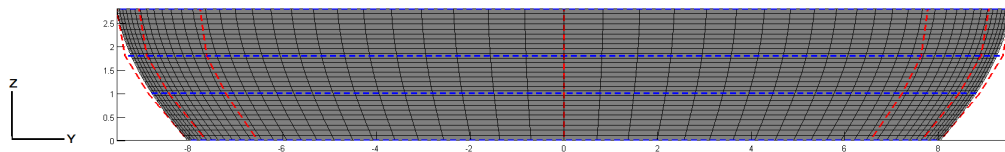
Figure 3.6: Front view of the 3D bow shape.

To calculate the flare angle, the buttock angle and the frame angle along the waterline (ice top surface) and the ice bottom surface, normal vectors have to be generated out from the NURBS surface along the two lines. The normal vectors will be generated out from a defined number of points along the waterline and the ice bottom surface, which are given by the parameters c and d. The points defined by c are generated along the waterline and the ice

bottom surface starting from point $x = 0.001$ and ending at point $X(3,3)$ and $X(2,3)$, respectively. To include the starting point when calculating the angles along the lines, the starting point is defined to be $x = 0.001$ for both waterline and ice bottom surface. If the starting point was defined as $x = 0$ it would be excluded due to little accuracy in the function which locates the points on the surface. The parameter d will generate points from $X(3,3)$ to $X(3,4) - 0.1$, and from $X(2,3)$ to $X(2,4) - 0.1$ for the waterline and the ice bottom surface respectively. The ending points are intentionally chosen not to be the control points X(3,4) and X(2,4) as these points do not need to be considered since they are both depending on the given stem angle, which is already given as a parameter in the model. The generation of points along the surface is given by two parameters to be able to obtain more points in the foremost part of the bow, which has the largest curvature and thereby calculate the average angles of the bow shape more correctly.

An illustration of the parametric model in port side view including the points for $c = 21$ and $c = 19$ and the normal vectors along the waterline and the ice bottom surface, can be seen in Figure 3.7.
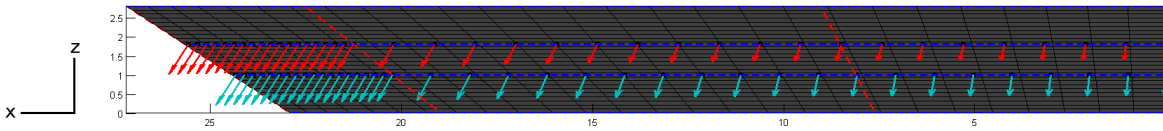
Figure 3.7: Port side view of the 3D model with generated normal vectors out from the NURBS surface.

To obtain a complete bow shape, the parametric model has to consider an additional 2-by-4 mesh grid which has to be added to the existing mesh grid describing the bow skeleton (see Appendix B.1, B.2 and B.3 for MATLAB code). The complete bow shape is only used for visualization, and thus it is not modelled in detail. An illustration of the complete bow shape is given in Appendix B.4.

As the model is parametric, it will be applicable for a wide variations of bow shapes, but the parameters can only be changed relative to each other to obtain a realistic bow shape, which means that there must be a certain ratio between the inserted values. The process of modelling realistic bow shapes was time consuming as each control point had to be adjusted by a testing and failing process in order to check how the bow skeleton would change with the parameters. This resulted in limitations for the input parameters and the model is therefore not valid for all values. The parameters are decided to be within the ranges given in Table 3.2, and the given ranges for L_{bow} and B, are based on dimensions from reference ships such as the icebreakers KV Svalbard, Otso and Tor Viking II.

To keep a realistic shape, it is not possible to combine a large α_1 with a small B and large α_2, and neither can a small α_1 be combined with a large B, and a small α_1 with a small α_2. The B/L_{bow} ratio should be between 0.5 and 0.9 to obtain a reasonable bow shape, which is based on the B/L_{bow} ratio of the reference ship KV Svalbard having a modern icebreaking bow.

Table 3.2: Limitations for the parametric values in the model.

Parameter	Range
L_{bow} [m]	[20,40]
B [m]	[15,30]
α_1 [degree]	[25,89]
α_2 [degree]	[1,5]
β_1 [degree]	[70,80]
β_2 [degree]	[40,60]
φ [degree]	[20,90]

3.3 Description of the MATLAB code

The main file, "runModel.m", developed in MATLAB is split into four main sections; the first section in the script contains the input parameters, the second section is calling the different sub-routines, created as functions, the third section calculates and displays the results, and the fourth and last section presents the plotting. If the whole bow shape is considered, an additional section (referring to Appendix B.1) is added in the script containing the function calls and the plotting of the additional mesh grid and NURBS surface. The parameters defined in the main file are presented in Table 3.3.

Table 3.3: Variables and constants used in the 3D parametric model.

Parameter	Explanation	Unit
H_1	Height from z=0 to ice bottom surface	m
H_2	Height from waterline to top of bow	m
H_3	Height from z=0 to top of bow	m
L_{bow}	Length of bow (along x-axis)	m
B	Breadth of ship (along y-axis)	m
T_b	"Draught", height from z=0 to ice top surface (along z-axis)	m
α_1	Waterline entrance angle close to the stem	degree
α_2	Waterline entrance angle close to the exit	degree
β_1	Frame angle above ice top surface	degree
β_2	Frame angle under ice top surface	degree
φ	Stem angle	degree
h_i	Ice thickness	m
c	Number of points on NURBS surface between $x = 0.001$ and $X(2:3,3)$	-
d	Number of points on NURBS surface between $X(2:3,3)$ and $X(2:3,4)-0.1$	-
$degree$	Degree of polynomial function	-
h	Step size in cental difference scheme	-
$direction$	Ray casting direction (basis vector)	-
ns	Number of points on NURBS surface in s-direction	-
nt	Number of points on NURBS surface in t-direction	-
s	Array of points on NURBS surface in s-direction	-
t	Array of points on NURBS surface in t-direction	-
$weights$	Weights of control points	-

The degree of polynomial function, $degree$, is chosen to be equal to $3 + 1$, the step size, h, is 0.0001 and the ray casting direction, $direction$, is $[0, 1, 0]$.

The structure of the MATLAB code is represented in a flow chart illustrated in Figure 3.8. "runModel" is representing the main file of the model which is calling up predefined functions and thereby generating a 3D bow shape. The rectangular boxes are representing the function files (.m-files) created in MATLAB, while the elliptical boxes are representing the definition of parameters, the results, and the plotting by applying integrated functions in MATLAB. The blue characters in Figure 3.8 are indicating the output parameters and the red characters are indicating the input parameters. The main file, "runModel.m", file is given in Appendix C, together with the belonging functions, where the parameters used in every function and a more descriptive explanation of each file is given together with the file.

"ControlPoints" is the function generating the bow skeleton consisting of control points in a mesh grid as discussed in Section 3.1. The function "RayNurbsIntersection" will take in the defined control points in the previous function, together with the defined points along the ice top surface and the ice bottom surface. An initial point, $p0$, will be defined at the x-axis in addition to an initial variable vector, $rst0$, which will point towards the y-direction. A minimum search function is used to locate the points on the ice top surface and the ice bottom surface given at the NURBS surface. To locate the points, there will be defined points on the ray and points on the NURBS surface. The goal is to change rst until the length of XA (which is a vector pointing from a point on the NURBS surface towards the point located on the ray) is equal to zero. This means that the point on the ray and the point on the surface will coincide, and thus the intersection point is found.

"RayNurbsIntersection" will call "SurfaInterpolationGrid" in order to compute the intersection between the casted ray and the NURBS surface. "SurfaInterpolationGrid" will compute points on the NURBS surface by using the control points (cpX, cpY, cpZ) and the parameters s and t, which will move along the surface. "SurfaInterpolationGrid" will generate Xst, Yst and Zst, which are the 3D positions of the NURBS surface at the position of s and t.

"SurfaceNormals" computes the normals out from the NURBS surface in the generated points along the ice top waterline and the ice bottom surface by using central difference scheme. It is called by using the defined s- and t-positions of the generated points along the surface, and it will use central difference scheme to .

The function "BowShapeAngles" will simply calculate the bow shape angles in the generated points by using the defined normal vectors in the function "SurfaceNormals". The angles are estimated by projecting the normal vectors down on the considered plane. The average angles for waterline entrance angles and buttock angles, are found by considering the equidistant between the points in the x-direction. For the average waterline entrance angle this will be somewhat incorrect as the distance in the y-direction is not considered. This means that the computed average waterline entrance angle in the model for a wedge-shaped bow versus a spoon-shaped bow would probably be somewhat misleading.

As mentioned already, the surface will be generated by "SurfaceInterpolationGrid", and "SurfaceInterpolationGrid" will call on "BSplineBasis", which will generate the splines that the NURBS surface consists of as presented in Section 3.2. "BSplineBasis" will make the B-splines Bs and Bt by using the integrated function "spcol" in MATLAB.

The last function "GridPlot" is generating the mesh grid made out of the control points cpX, cpY and cpZ, which defines the bow skeleton. In order to generated the scatter plotting of the control points and the points defined along the ice top surface ice top bottom, in addition to a coloured NURBS surface, integrated plot-functions are applied in MATLAB.
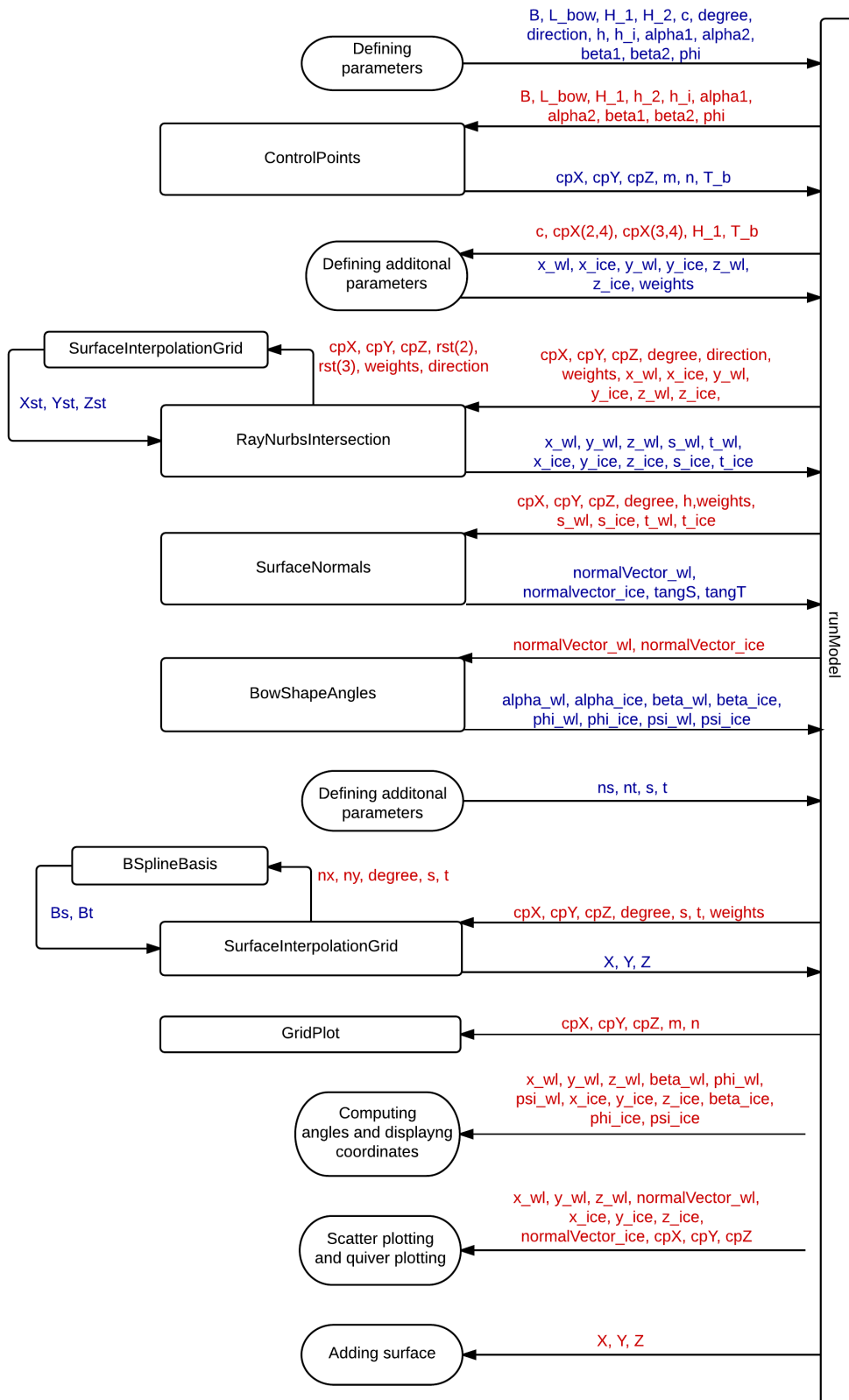
Figure 3.8: Flow chart of the MATLAB code.

4. Sensitivity Analysis

A sensitivity analysis is performed in order to identify how a change of the bow geometry will affect the breaking resistance. The sensitivity study is performed on selected ice resistance prediction methods, and the developed bow shape modelling tool will be applied in order to visualise the bow shapes and to help identifying the sensitivity of the methods. In addition, the combinations of the bow shape angles giving the lowest breaking resistance will be found. The methods to be compared are both considering the same bow shape angles and can be applied to estimate the breaking resistance. The selected methods for the sensitivity study are therefore the semi-empirical method of Lindqvist (1989) and the newly developed numerical method of Erceg et al. (2014).

To have a starting point, the data from a reference ship is used to set the main dimensions, and the bow angles are adjusted to obtain different bow shapes. In this analysis, the focus is set towards the average waterline entrance angle, α_{avg}, and the average buttock angle, ϕ_{avg}, the flare angle, ψ, and the ship beam, B. The investigated α and ϕ are seen as average values in this Chapter as the method of Lindqvist is considering single value of each bow angle. The sensitivity of the results related to the ice thickness are out of scope of this thesis and the ice thickness will therefore be kept constant during the sensitivity study. This also applies for the ice properties.

The ship data used in the methods are retrieved from the icebreaker KV Svalbard (referring to Table 3.1) and the data of the ice properties is decided to be the same as used in the comparison of the semi-empirical and numerical method in section 2.8, Table 2.4b. An overview of the input data used in the methods is given in Table 4.1, where Table 4.1a includes the ship parameters for KV Svalbard and Table 4.1b presents the values for the additional parameters used in the applied methods.

The input parameters for the parametric model in MATLAB are given in Table 4.2. To obtain the desired average bow angles, α_1 and φ have to adjusted until the desired average angles are found within the given ranges. However, the limitations of the parametric model discussed in Section 3.2 must be kept in mind when combining the values of the parameters.

Table 4.1: Input data for the applied methods.

(a) Ship parameters.

Parameter	KV Svalbard
L_{pp} [m]	89
L_{bow} [m]	27.24
B [m]	19.1
T [m]	6.5

(b) Additional parameters.

Parameter	Value
h_i [m]	0.75
σ_b [kPa]	550
ρ_i [tonnes/m^3]	0.900
ρ_w [tonnes/m^3]	1.025
g [m/s^2]	9.81
E [kPa]	$2 \cdot 10^6$
μ [-]	0.1
ν [-]	0.3

Table 4.2: Input parameters for the parametric model.

Parameter	Value/Range
α_1 [deg]	[20,89]
α_2 [deg]	3
β_1 [deg]	80
β_2 [deg]	55
φ [deg]	[20,90]
c [-]	21
d [-]	19
H_1 [m]	1
H_2 [m]	1

To compare how the breaking resistance will be affected by certain bow shapes, two characteristic bow shapes will be used as a case study bows. The first bow shape will be a wedge-shaped bow with small waterline entrance angle and the second bow shape is the spoon-shaped bow, which has a larger waterline entrance angle at the stem. Hereafter, the wedge-shaped bow is denoted as bow shape 1, and the spoon-shaped bow is bow shape 2. The bow shape angles for bow shape 1 are α = 25 and ϕ =30, while for bow shape 2, the angles are α = 44 degrees and ϕ = 25 degrees. Bow shape 1 can be seen in Figure 4.1 and bow shape 2 is seen in Figure 4.2
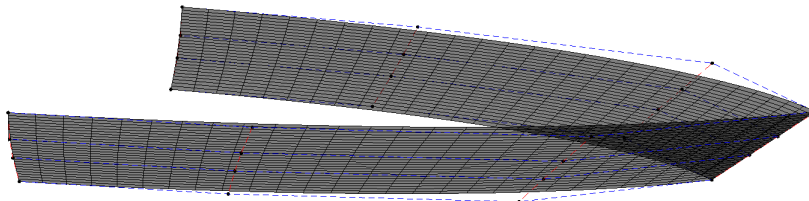
Figure 4.1: Bow shape 1: Wedge-shaped bow.
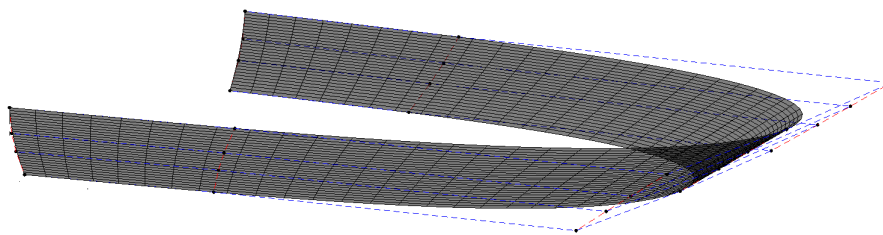
Figure 4.2: Bow shape 2: Spoon-shaped bow.

4.1   Application of the Method of Lindqvist

Lindqvist (1989) has defined the breaking resistance to consist of crushing (Equation 2.5) and bending (Equation 2.8) of ice, and the breaking resistance is thus given as

$$R_{br} = R_c + R_b \tag{4.1}$$

The resulting resistance is depending on the waterline entrance, α, and the buttock angle, ϕ, and the results are illustrated in Figures 4.3, 4.4 and 4.5. The results are normalized and thus a relative comparison of the results is performed. The colour bar is indicating the relative breaking resistance, while the green coloured point indicates bow shape 1 and the cyanide coloured point indicates bow shape 2. The buttock angle is given along the x-axis and the waterline entrance angle is given along the y-axis, while the breaking resistance is given along the z-axis.
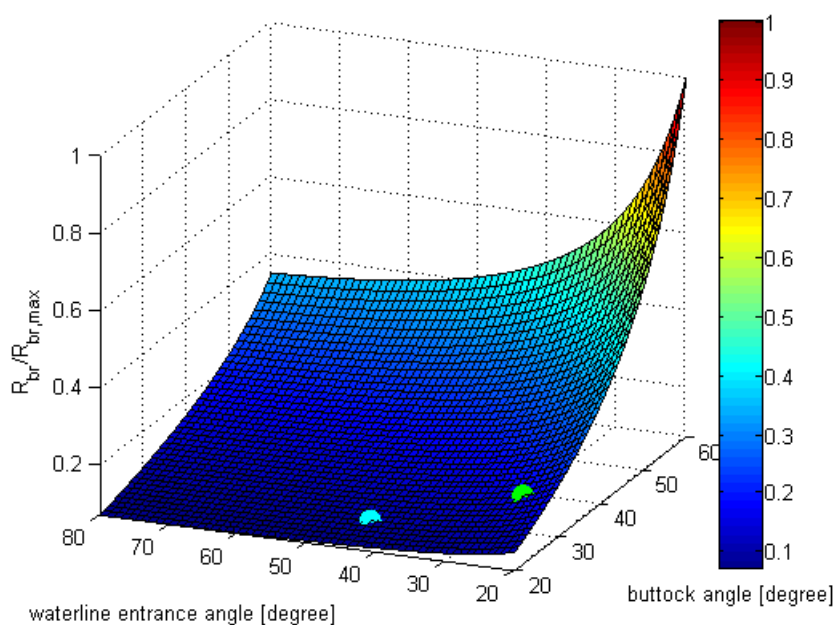
Figure 4.3: Relative breaking resistance versus waterline entrance angle and buttock angle after applying the method of Lindqvist.
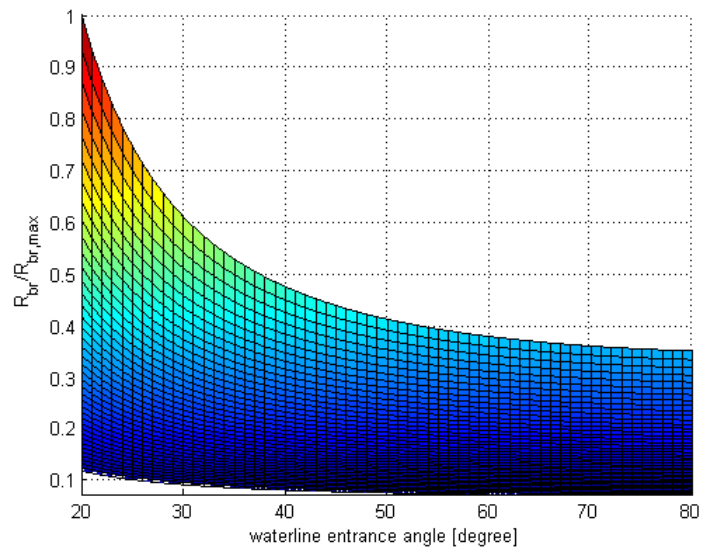
Figure 4.4: Relative breaking resistance seen in the yz-plane after applying the method of Lindqvist.
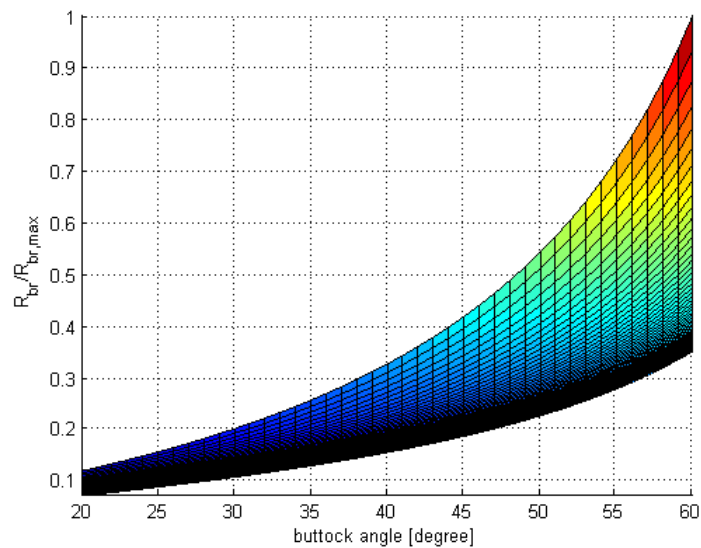
Figure 4.5: Relative breaking resistance seen in the xz-plane after applying the method of Lindqvist.

From Figures 4.3, 4.4 and 4.5 it can be seen that an increasing buttock angle will result in an increasing resistance, while an increasing waterline entrance angle will result in a reduced resistance, which means that a combination of a high buttock angle and a low waterline entrance angle will give high breaking resistance.

The relative breaking resistance seems to increase faster in the range of $\alpha \; \epsilon [20,50]$ and ϕ $\epsilon [40,60]$. In general, the breaking resistance seems to be more sensitive to a change of the buttock angle compared to a change of the waterline entrance angle.

As seen in Figure 4.3, the relative breaking resistance for bow shapes 1 and 2 are quite similar. It can also be seen that for several combinations for the buttock angle and the waterline entrance angle, the resulting breaking resistance will be the same. Table 4.3 shows the relative breaking resistance for certain combinations of buttock angles and waterline entrance angles. For example, the relative breaking resistance equal to 0.35 is given for ϕ = 60 degrees and α = 80 degrees, and for ϕ = 47 degrees and α = 26 degrees. For α, this is a difference of 54 degrees, which is a significant step as the bow shape will look spoon-shaped (or more like a landing craft bow) for α = 80 degrees, while being wedge-shaped for α = 26 degrees. The ϕ will however not change more than 13 degrees for the same angle combinations.

Table 4.3: The resulting breaking resistance presented with regard to combinations of buttock angle and waterline entrance angle.

ϕ [degree]	α [degree]	$R_{br}/R_{br,max}$
24	80	0.086
22	48	0.086
20	36	0.086
22	20	0.134
32	44	0.133
34	56	0.133
60	80	0.351
47	26	0.350
49	21	0.485
60	39	0.484
53	20	0.641
59	27	0.640

As the breaking resistance consist of two components, crushing and bending, it is interesting to look at how the two components are influencing the breaking resistance, and how the two components will be affected by the buttock and the waterline entrance angle. The bending and crushing components are plotted separately against both of the angles. The relative bending and the crushing resistance to the breaking resistance are illustrated in Figure 4.6, where Figures 4.6a, 4.6c and 4.6e illustrates the relative bending resistance presented in different planes, and Figures 4.6b, 4.6d and 4.6f illustrates the relative crushing resistance seen in different planes.
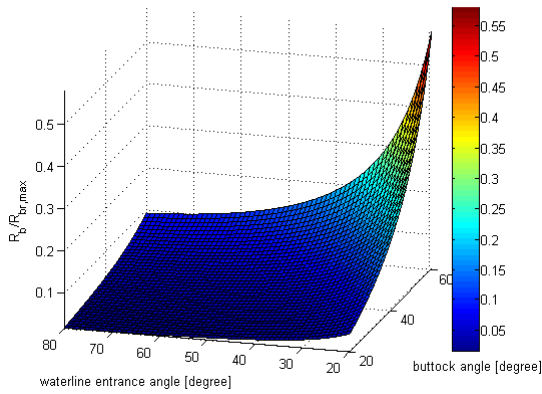
(a) Relative bending resistance.
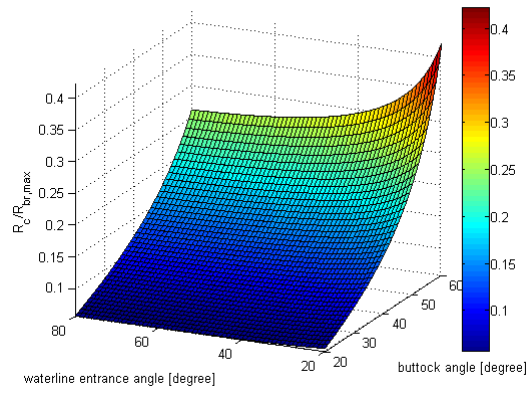
(b) Relative crushing resistance.
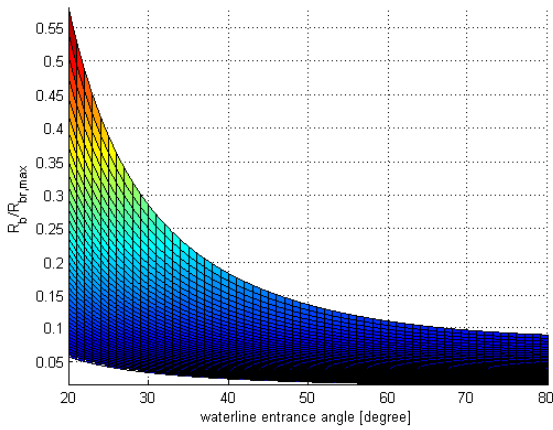
(c) View of relative bending resistance in yz-plane.
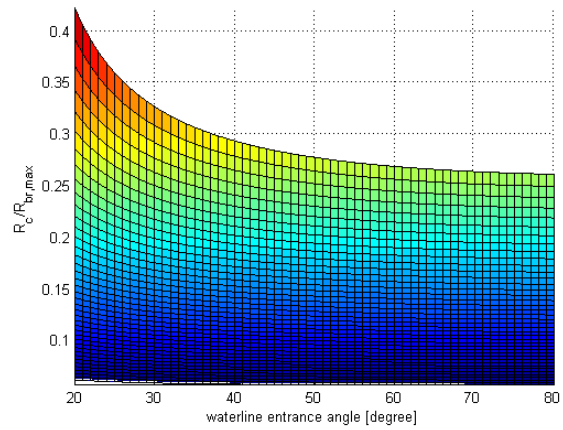
(d) View of relative crushing resistance in yz-plane.
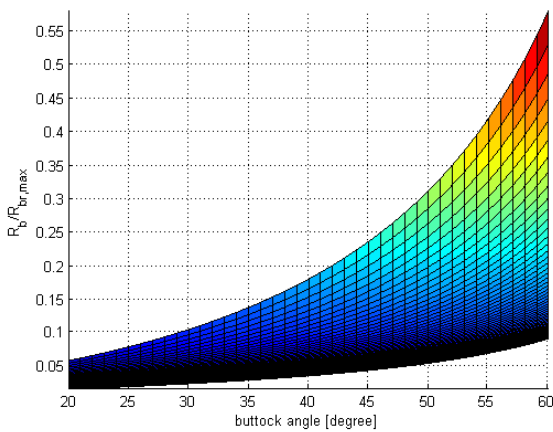
(e) View of relative bending resistance in xz-plane.
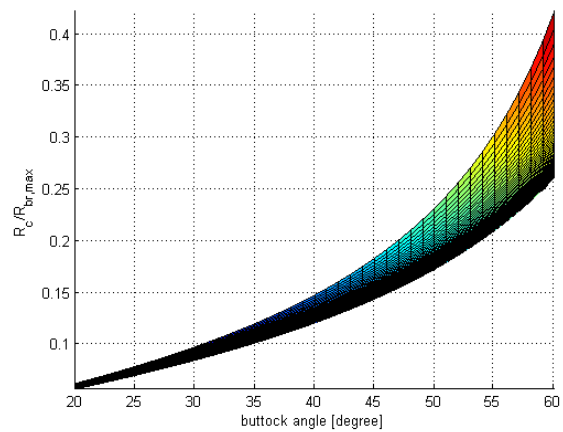
(f) View of relative crushing resistance in xz-plane.

Figure 4.6: Bending and crushing resistance versus buttock angle and waterline entrance angle after applying the method of Lindqvist.

Figures 4.6a, 4.6c and 4.6e indicate that the bending resistance will be more sensitive for $\alpha \in$ [20,40] and for $\phi \in$ [35,60]. For the crushing resistance, it can be seen from Figures 4.6b, 4.6d and 4.6f that for an increase in the buttock angle the resistance will increase significantly compared to a decreasing waterline entrance angle. Due to the presented results it can be concluded that the bending resistance is sensitive to both the waterline entrance angle and the buttock angle when the waterline entrance is in the range of 20 to 40 degrees and the buttock angle is in the range of about 35 to 60 degrees, and the crushing resistance is clearly more sensitive to a change in the buttock angle.

To find out how the breaking resistance will change with the flare angle, ψ, the change of the flare angle relative to the waterline entrance angle and the buttock angle has to be identified first, which can be seen in Figure 4.7, where the colour bar indicates the value of the flare angle.
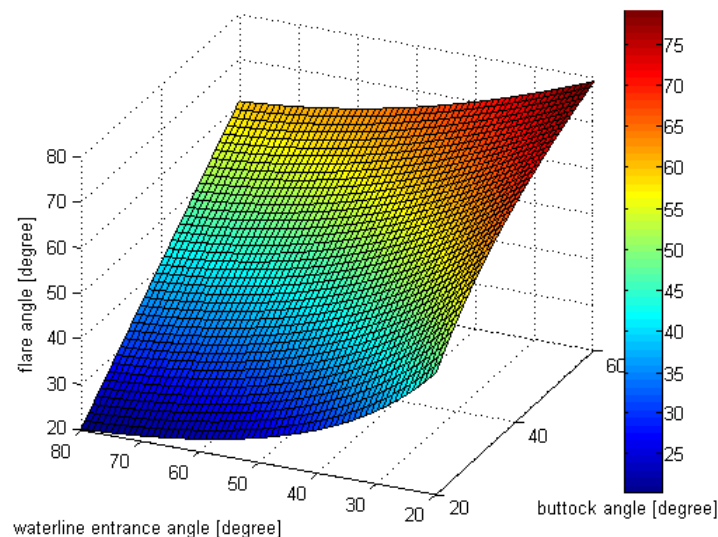
Figure 4.7: Influence of waterline entrance angle and buttock angle on the flare angle.

From Figure 4.7 it can be seen that the flare angle will increase for an increasing buttock angle and a decreasing waterline entrance angle, which means that an increased flare angle will give an increased breaking resistance according to Lindqvist's method.

Until now the focus has been set towards the effect of bow shape angles on the breaking resistance, but as previously discussed an additional ship parameter will affect the resistance, which is the ship beam. When the values for the waterline entrance angle and the buttock angle are set, the breaking resistance will increase for an increased ship beam as the bending resistance is linearly depending on the ship beam (see Equation 2.8). However, it is interesting to see how the ship beam will affect the breaking resistance with regard to α and ϕ.

For ϕ = 30 degrees, the resulting plot for the breaking resistance versus ship beam and waterline entrance angle is given as shown in Figure 4.8 (left), while for α = 59 degrees and a varying ϕ, the results are given in Figure 4.8 (right). From the left figure in Figure 4.8, it is seen that the relative breaking resistance will increase faster with regard to the *B* for α <

35 degrees. For α=80 degrees, an increase in the beam will increase the relative resistance with 0.01, and for α = 20 degrees, and increase in the beam will increase the relative resistance with 0.04. From the right figure in Figure 4.8, it can be found that for ϕ = 20 degrees, an increase of B will increase the relative resistance with 0.01, while for ϕ = 60 degrees, the increasing B will increase the relative breaking resistance with 0.05.
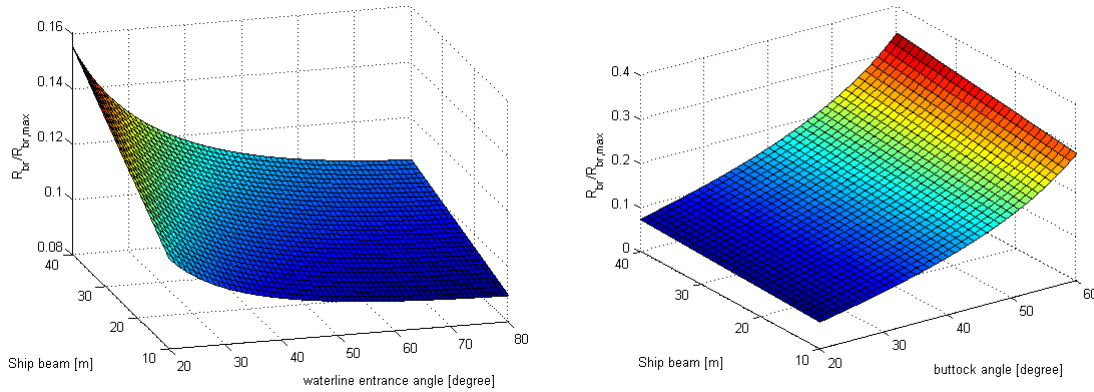
Figure 4.8: The breaking resistance versus ship beam, waterline entrance angle and buttock angle after applying the method of Lindqvist.

4.2   Application of the Method of Erceg et al.

The method of Erceg et al. is modelling the initiation of icebreaking pattern in level ice through a simulation procedure. By applying the parametric model in the method, the icebreaking pattern for a desired bow shape can be identified. The method will call on the parametric model and use the coordinates of the points generated along the ice top and the ice bottom surface, the ice thickness, and the computed bow shape angles at T_b, to simulate a ship penetrating the ice edge. The obtained results from the simulation will be given as total breaking resistance.

As the method is newly developed and not tested in a larger extent, a sensitivity analysis will be performed to identify how the breaking resistance is affected, not only by changing the bow geometry, but also the step size and the length of the simulation.

The first step was to perform a convergence study in order to decide which simulation step, x_{step}, and simulation length, x_{end}, to use for the further sensitivity study, and thereby also see the effect of the time step on the final result. The rest of the parameters were kept constant during this convergence study in order to isolate the influence of x_{step} and x_{end}.

The instantaneous ship-ice interaction forces will increase until the ice cusp is broken off from the ice edge. Therefore, these ice interaction forces will fluctuate during the penetration of the ice edge due to repetitive cycles of ice cusps breaking off (see Erceg et al. (2014). For a small simulation step, it was easier to observe this process on the resulting plot of the instantaneous breaking resistance as the ice loads were better captured. It was observed that the average of the instantaneous forces (the total breaking resistance), R_b, would change for

an increased simulation length and a constant simulation step due to more ship-ice interaction zones developing once the initial ice edge has been penetrated deep enough.

When the simulation length gets large enough, the R_b will converge to be constant. The convergence test can be seen in Table D.1, Appendix D and it was found that the step size and the length of the simulations that will be used for the sensitivity study, will be 0.1 m and 265 m, respectively.

The next step was to run simulations for several types of bow shapes, and the simulation results can be seen in Appendic E, Table E.1. To obtain average waterline entrance angles and buttock angles, the following parameters had to be adjusted (as the parameters are not average values): α_1, α_2, φ and $radScale$. Figure 4.9 illustrates the results obtained from the simulations. The red points are the specific combinations of the average bow angles, and there is a surface interpolated between the points to better visualise the results. Also in this figure, the green coloured point and the cyanide coloured point are illustrating bow shape 1 and 2, respectively. It was not possible to simulate bow shape 2 due to errors occurring in the simulation, but the point is assumed to be placed as shown in Figure 4.9 based on the results obtained from other similar bow shapes. The coloured bar in the figure indicates the relative breaking resistance.
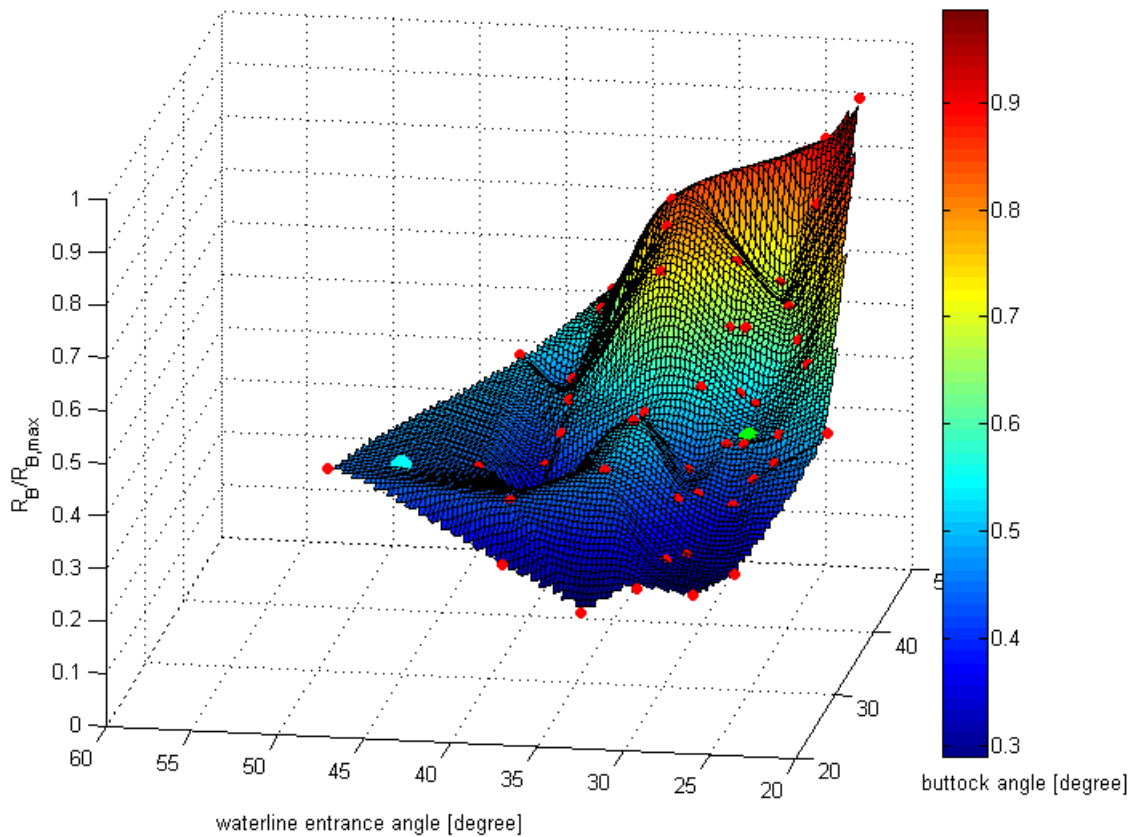
Figure 4.9: Relative breaking resistance versus waterline entrance angle and buttock angle after applying the method of Erceg et al.

From Figure 4.9 it is observed that the breaking resistance will be high for combinations of small waterline entrance angles and large buttock angles, and the overall trend of the plot seems to be reasonable. However, the points are quite scattered and it can clearly be seen that there are certain points that deviate from the rest of the points.

5. Discussion and Conclusion

5.1 Semi-Empirical and Numerical Methods

From the literature study, it was found that a typical icebreaking bow is rounded and features a small buttock angle, which will bend and break the ice efficiently while reducing the crushing as the bow will ride up onto the ice. It is also desired that the bow has a larger waterline entrance angle, which will contribute to better ice clearing efficiency.

The parameters considered in the semi-empirical ice resistance prediction methods were not common for all methods (see Table 2.2). The methods of Kashteljan et al. (1969), Enkvist (1972) and Vance (1975) developed in earlier times, were simple and quite similar to each other with regard to considered parameters. However, none of the three methods are considering parameters describing the bow shape, but as the methods are all considering empirical values, the values may be based on one or several different bow shape, usually used in their development. This means that the methods will be insensitive to a change of the bow geometry, and thus they are not suitable to apply when computing the ice resistance on ships with different bow characteristics. In spite of this, it is important to point out that the early developed methods have contributed greatly to the knowledge about the icebreaking process and to further development of ice resistance prediction methods. In the newer methods, there can therefore be identified similarities to the old methods, such as the decomposing of the ice resistance.

Semi-empirical approaches presented in this thesis developed in the last decades, are the methods of Lindqvist (1989), Riska et al. (1997) and Keinonen et al. (1991, 1996). The three methods are all considering parameters describing the bow shape (referring to Table 2.2), but Riska et al. will only consider one bow angle, which is the stem angle. In addition, the method is considering seven constants, which are based on the performance of ten merchant ships navigating in Baltic ice conditions, which had a waterline entrance angle ranging from 19 to 40 degrees. The constants will thereby justify for the exclusion of parameters describing other bow angles in the mathematical expression for ice resistance. Moreover, the ice density, ice bending strength and friction coefficient are kept constant in the method of Riska et al. as the ships were navigating in similar ice conditions. Due to this, the method might not give the most reliable results when applied to ships navigating in different ice conditions than in the Baltic. In addition, it may not be the best method to apply for ships with larger waterline entrance angle than 40 degrees, such as a spoon-shaped bow or a landing craft bow.

The methods of Lindqvist, Keinonen et al. and Riska et al. were found to give similar ice resis-

tance for the icebreaker KV Svalbard (see Figure 2.6), but for the ice-capable merchant vessel Sotka (see Figure 2.7), the results would deviate more, especially for Lindqvist. Lindqvist seemed to be more sensitive to a change of the ship size and the bow angles as the method would give significant higher ice resistance for Sotka compared to the other two methods. Keinonen et al. gave a small increase in the ice resistance for Sotka, while Riska et al. would give a slightly higher increase of the ice resistance, and thus these two methods do not seem to be sensitive to a change of the bow geometry. However, the results obtained from these two methods might have been different for ships with a significant change in the buttock angle as they both are considering this parameter.

It is important to point out that the obtained results shown in Figures 2.6 and 2.7 from the applied methods are based on data from only two different ships, and that the ice properties are set to be the same in the computed ice resistance curves. In reality the ice is non-uniform and the ice properties will vary with regard to season and geographical areas. Furthermore, the results proved that the computed ice resistance will change for ships with different size and bow shape as the ship parameters are considered in the methods. Hence, from the achieved results, it can be concluded that maybe some of the semi-empirical mathematical models are not valid for all kinds of ship sizes and shapes.

There will always be uncertainties connected to the results as the presented methods are including some common parameters, and based on diverse assumptions. In addition, the methods are validated against full-scale measurements for ships of different sizes and bow shapes operating in various geographical areas. Due to the underlying assumptions and validation of the methods, the applicability of the methods will be limited, and they should be applied with caution.

The main difference between the numerical methods for ice resistance prediction presented in this thesis, was found to be the predefinition of the ice cusp geometry. The methods of Liu et al. (2006), Sawamura et al. (2009), Lubbad and Løset (2011) and Su et al. (2010) were defining the cusp shape as specific, while Erceg et al. (2014) developed a method that will obtain irregular ice cusp shapes. The drawback of the methods defining specific ice cusp shapes, might be exclusion of other ice cusp shapes formed during the icebreaking process. This can give misleading prediction of the icebreaing pattern, and thus the ice resistance, which is strongly related to icebreaking pattern. Due to this (and as the method was provided), the method of Erceg et al. was chosen to be applied for the sensitivity study.

In general, the main point that separates the semi-empirical and the numerical methods, is the consideration of physical effects of the icebreaking process and thereby the predefinition of the ice cusp geometry. The semi-empirical approaches will identify the contributions of the resistance components, but the components are not measured over time, which may cause inaccurate results. By having knowledge about how the ice will break off when in contact with the ship hull, the interpretation of the ice resistance can be improved. The ice cusps breaking off the ice edge are highly depending on the bow geometry (Myland and Ehlers, 2014), and thereby the numerical methods can give more reliable results compared to the semi-empirical approaches.

5.2 Sensitivity Analysis and Parametric Model

The methods selected to be used for sensitivity analysis were the methods of Lindqvist (1989) and Erceg et al. (2014). The methods can predict the breaking resistance and they are both considering parameters describing the bow shape in form of waterline entrance angle and buttock angle. The method of Erceg et al. simulates a ship advancing in level ice and thus give the total resistance forces over a time period, which differs from Lindqvist.

The method of Lindqvist seems to be less sensitive to the waterline entrance angle, but when the buttock angle is increased, the relative breaking resistance will increase for small waterline entrance angles (see Figure 4.4). This might indicate that the method of Lindqvist is limited to wedge-shaped bows, which are characterised by a smaller waterline entrance angle.

As seen in Figure 4.6, the breaking resistance consists of a crushing and a bending component, and the bending component seemed to be more sensitive for smaller waterline entrance angles and larger buttock angles, while the crushing component is more sensitive to a change of the buttock angle. This was to expect as a small buttock angle will give less crushing, which means that the ship will rather ride upon the ice than crushing the ice, and a large buttock angle will result in an increased crushing resistance due to a more vertical bow shape.

In addition, it was found that an increasing flare angle was resulting in an increasing breaking resistance (referring to Figure 4.7), and it can thus be desired to have a small flare angle to reduce the breaking resistance, which means a combination of a large waterline entrance angle and a small buttock angle. The last parameter considered with regard to the bow geometry, was the ship beam. In general, the effect of the ship beam on the relative breaking resistance would not be significant compared to the effect of the bow angles on the breaking resistance (see figure 4.8).

The overall trend of the results obtained from the method of Erceg seems to be as expected as higher buttock angle and smaller waterline entrance angle will give higher breaking resistance, which can be seen in Figure 4.9. However, there are some points in the results that are deviating and seems to be incorrect, which can be caused by limitations in the parametric model. In order to check if the results (which appeared to be incorrect) were simulated with wrong input data, new simulations were performed for the same average angles. However, the results remained the same, and therefore there was no mistake made when entering the input values into the simulation procedure. It is also important to keep in mind that the different combinations of the bow angles can give the same average values, and that the bow shapes thereby do not necessarily give the same results.

If the results obtained from the two different methods are compared with regard to bow shape 1, which is a wedge-shaped bow (see Figure 4.1), and bow shape 2, which is a spoon-shaped bow (see Figure 4.2), Erceg will give a higher relative breaking resistance for bow shape 1 compared to the results obtained by Lindqvist. The results for bow shape 2 was not obtained for the method of Erceg as there occurred an error in the simulation. However, it can be assumed that Erceg will give higher relative breaking resistance for bow shape 2 compared to Lindqvist based on the results from the average values of other similar bow shapes.

This might indicate that the method of Erceg is more sensitive to a wider diversity of bow angles compared to the method of Lindqvist.

The combinations of the bow shape angles resulting in the lowest resistance from Lindqvist was given to be a waterline entrance angle equal to 80 degrees and a buttock angle equal to 20 degrees, which will be a landing craft bow. After applying the method of Erceg, the lowest breaking resistance from the simulation was for a waterline entrance of 32 degrees, and a buttock angle of 18 degrees, which is a bow between a wedge-shaped bow and a spoon-shaped bow. This is a quite large difference for the waterline entrance angles, but can be explained by the uncertainties occurring in both the parametric bow model and the simulations, and also the limitations of the parametric bow model and the method of Erceg. However, this can also indicate that the method of Erceg is applicable for a wider diversity of bow shapes compared to the method of Lindqvist as Erceg is considering the physical effects of the icebreaking process. The bow shapes resulting in the lowest breaking resistance from each method can be seen as the best shapes for the breaking resistance, but those bow shapes might not be the best bow shapes for the total ice resistance since only the breaking component is considered in this sensitivity analysis.

During the simulations of the different bow angles, there occurred errors for certain combinations of angles, which limited the investigated ranges of the bow angles. The errors seemed to occur frequently for high average waterline entrance angles and high average buttock angles. In addition, there also occurred errors in the code of the parametric model. As previously discussed, the parametric model is not applicable for all input values. The limitations are given for a large α_1, which can not be combined with a small ship beam or a large α_2. A small α_1 combine with a large beam should also be avoided. Another limitation of the parametric model, is the distance of the NURBS surface to the control points. For the parts of the surface with larger curves, the distance to the control points will increase. This means that an increased value of α_1 will not necessarily give the desired shape, such as a spoon-shaped bow. This also means that a landing craft bow cannot be obtained neither. Further, the estimated calculated average angles in the generated points along the ice top surface and the ice bottom surface are estimated based on the distance given in x-direction. The estimated average waterline entrance angle along the surface will therefore be inaccurate as the distance in the y-direction is not considered. Since the y-coordinates of the points were calculated based on an intersection method, the points would not be equidistant in the y-direction. For further work, it is recommended to change this in order to obtain more accurate average values.

5.3   Conclusion

The method of Lindqvist was found to be more sensitive for an increase in the buttock angle with regard to the breaking resistance, but the method was also found to be sensitive for smaller waterline entrance angles combined with larger buttock angles. A small flare angle results in lowest breaking resistance, according the results obtained by the method of Lindqvist. Furthermore, the change in the ship beam will not affect the breaking resistance significantly, and thereby the method of Lindqvist is not highly sensitive to a change of the ship beam.

The methods of Lindqvist and Erceg are in overall giving results in the same trend as a small waterline entrance angle and a large buttock angle will in both of the methods result in a larger relative breaking resistance. However, the method of Erceg seems to be more reliable and sensitive to the bow shape angles as it considers the physical effects of the icebreaking process. When applying Lindqvist, the bow found to be resulting in the minimal ice resistance, is a bow with maximum waterline entrance angle and minimum buttock angle in the considered ranges of the angles, which in reality will not be the best bow shape as other factors are not considered. Thereby the method of Erceg will give more reliable results compared to the method of Lindqvist.

According to the estimated average angles, the parametric bow model is only applicable for bow shapes with an average waterline entrance angle up to around 45 degrees, which will be a bow shape somewhere between a wedge-shaped bow and a spoon-shaped bow. The bow model is also limited to an average buttock angle up tp 60 degrees. It must be kept in mind that this will therefore cause uncertainties in results achieved for large average waterline entrance angles and thereby the results have to be considered with a critical view. The method of Erceg seems to less applicable for especially large waterline entrance angles and large buttock angles. However, according to the results obtained from the simulations, it seems to be limited to average waterline entrance angles from 20 to 50 degrees, and average buttock angles from 20 to 45 degrees. This certain range can be caused by the limitations of the parametric bow model.

6.   Further Work

The developed parametric model in MATLAB is able to generate desired bow shapes as it is based on parameters describing the bow shape, such as the bow length and breadth, and the angles describing the curvature. However, the model is only considering the ice belt, and not the top or bottom of the bow. It can be desired to see the whole bow shape to get a better visualization, and to be able to include an optional bow plough and thereby also consider the underwater part, which affect the submersion resistance. As the model is now, it is possible to add the bottom of the bow by including an additional mesh grid deciding the shape, but this mesh grid is including too few control points in order to give a correct picture of the bottom. Therefore, this can be further developed to obtain a more realistic bottom of bow.

Further, there can be performed a thorough diagnostic of the functions made in the MATLAB code to identify the source of errors occurring for certain combinations of the input parameters describing the bow shape angles. The problem was attempted to be detected, but without success. Another improvement point of the model is to adjust the weighting of the control points to reduce the distance between the NURBS surface and the control points in order to be able to generate a wider diversity of bow shapes.

Due to time constraints, not enough time as spent on analysing and testing the method of Erceg et al. In further work, the method should be more thoroughly analysed, and further analysis that can be performed is to look at how the ship size will affect the resistance by playing with different combinations of ship beam, draught and bow length. In addition, the angle of the ice edge (which the ship penetrates), can be adjusted in order to identify if it will affect the final results.

As the sensitivity study performed in this thesis creates a basis for further investigation of the ice resistance, the next step can be to apply an optimization procedure for the applied methods. The aim of optimization procedure will be to minimize the ice resistance while keeping the open water resistance as low as possible. By performing this, the optimal bow shape angles for an icebreaking bow can be identified. This is quite extensive, and was thus not performed in this thesis.

Bibliography

Enkvist, E. (1972). On the ice resistance encountered by ships operating in the continuous mode of icebreaking. Report, The Swedish Academy of Engineering Sciences in Finland.

Erceg, S., Ehlers, S., und Polach, R. v. B., and Leira, B. (2014). A numerical model to initiate the icebreaking pattern in level ice. In *ASME 2014 33rd International Conference on Ocean, Offshore and Arctic Engineering*. American Society of Mechanical Engineers.

Institution, W. H. O. (2007). Beaufort gyre exploration project: Early icebreakers (20th century).

Institution, W. H. O. (n.d.). Icebreaker oden.

Jones, S. J. (2004). Ship in ice - a review. In *25th Symposium on Naval Hydrodynamics*.

Kashteljan, V., Poznjak, I., and Ryvlin, A. Y. (1969). *Ice resistance to motion of a ship*. Sudostroyeniye, Leningrad.

Keinonen, A. J., Borwne, R. P., and Revill, C. R. (1989). Icebreaker design synthesis analysis of contemporary icebreaker performance. Report, Report of AKAC Inc. to Transportation Development Centre.

Keinonen, A. J., Browne, R. P., and Revill, C. R. (1991). Icebreaker design synthesis: Phase 2: Analysis of contemporary icebreaker performance. Report, Report of AKAC Inc. to Transportation Development Centre.

Keinonen, A. J., Browne, R. P., Revill, C. R., and Reynolds, A. (1996). Icebreaker characteristics synthesis. Report, Report of AKAC Inc. to Transportation Development Centre.

Kerr, A. D. (1975). The bearing capacity of floating ice plates subjected to static or quasistatic loads - a critical survey. *Cold Regions Research and Engineering Laboratory*, 1:43.

Kjerstad, N. (n.d.). Development of ship design for ice navigation.

Kotras, T. V., Baird, A. V., and Naegle, J. W. (1983). Predicting ship performance in level ice. *Transactions of Society of Naval Architects and Marine Engineers (SNAME)*, 91:329–349.

Lau, M. and Derradji-Aouat, A. (2004). Preliminary modeling of ship maneuvering in ice. In *25th Symposium on Naval Hydrodynamics*.

Lindqvist, G. (1989). A straightforward method for calculation of ice resistance of ships. pages 722–735.

Lindstrom, C.-A. (1990). Numerical estimation of ice forces acting on inclined structures and ships in level ice. In *Proceedings of 22nd Offshore Technology Conference, OCT 6445*, pages 201–216. Offshore Technology Conference.

Liu, J., Lau, M., and Williams, F. M. (2006). Mathematical modeling of ice-hull interaction for ship maneuvering in ice simulations.

Lubbad, R. and Løset, S. (2011). A numerical model for real-time simulation of ship–ice interaction. *Cold Regions Science and Technology*, 65(2):111–127.

Meng, Y. and Jin, Y. (2011). *Bio-Inspired Self-Organizing Robotic Systems.* Springer.

Milano, V. (1973). Ship resistance to continuous motion in ice. In *SNAME Transactions 81*, pages 274–306.

Morley, J. P. (1962). Polar ships and navigation in the antarctic.

Myland, D. and Ehlers, S. (2014). Theoretical investigation on ice resistance prediction methods for ships in level ice. In *ASME 2014 33rd International Conference on Ocean, Offshore and Arctic Engineering*, pages V010T07A015–V010T07A015. American Society of Mechanical Engineers.

Naegle, J. N. (1980). *Ice-resistance prediction and motion simulation for ships operating in the continuous mode of icebreaking.* Thesis.

Nevel, D. E. (1958). *The narrow infinite wedge on an elastic foundation.* US Army Snow, Ice and Permafrost Research Establishment, Corps of Engineers.

Nevel, D. E. (1961). The narrow free infinite wedge on an elastic foundation. Report, DTIC Document.

Pospiech, P. (2013). New aker arctic oblique icebreaker.

Riska, K. (2011a). Design of ice breaking ships. *Course material NTNU*.

Riska, K. (2011b). Ship–ice interaction in ship design: Theory and practice. *Course Material NTNU*.

Riska, K., Leiviskä, T., Nyman, T., Fransson, L., Lehtonen, J., Eronen, H., and Backman, A. (2001). Ice performance of the swedish multi-purpose icebreaker tor viking ii. In *Proceedings of POAC*, pages 849–865.

Riska, K., Wilhelmson, M., Englund, K., and Leiviskä, T. (1997). Performance of merchant vessels in ice in the baltic. Report 52, Helsinki University of Technology.

Sawamura, J., Riska, K., and Moan, T. (2008). Finite element analysis of fluid-ice interaction during ice bending. In *Proceedings of the 19th IAHR Symposium on Ice*, pages 239–250.

Sawamura, J., Riska, K., and Moan, T. (2009). Numerical simulation of breaking patterns in level ice at ship's bow. In *Proceedings of 19th International Offshore and Polar Engineering Conference*, pages 600–607.

Schneider, P. and Eberly, D. H. (2002). *Geometric tools for computer graphics*. Morgan Kaufmann.

Sodhi, D. S. (1995). *Northern Sea Route Reconnaissance Study: A Summary of Icebreaking Technology*, volume 95. DIANE Publishing.

Su, B. (2011). Numerical predictions of global and local ice loads on ships.

Su, B., Riska, K., and Moan, T. (2010). A numerical method for the prediction of ship performance in level ice. *Cold Regions Science and Technology*, 60(3):177–188.

Tan, X., Su, B., Riska, K., and Moan, T. (2013). A six-degrees-of-freedom numerical model for level ice–ship interaction. *Cold Regions Science and Technology*, 92:1–16.

Valanto, P. (2001). The resistance of ships in level ice. *Transactions-Society of Naval Architects and Marine Engineers*, 109:53–83.

Vance, G. P. (1975). A scaling system for vessels modeled in ice. *Proc. SNAME Ice Tech. Symposium*, page 28pp.

Wang, S. (2001). A dynamic model for breaking pattern of level ice by conical structures. *ACTA POLYTECHNICA SCANDINAVICA, Mechanical Engineering*, 156.

Appendices

A. NURBS

This Appendix includes additional mathematical expressions for NURBS curve and surface. The expressions given here are integrated in a function in MATLAB named "spcol".

A B-spline rectangle patch is given as

$$X(s, t) = \sum_{i_0=0}^{n_0} \sum_{i_1=0}^{n_1} B_{i_0,j_0}^{(0)}(s) B_{i_1,j_1}^{(1)}(t) P_{i_0,i_1} \tag{A.1}$$

where $s\epsilon[s_0, s_{n_0}]$, $t\epsilon[t_0, t_{n_1}]$, $1 \leq j_0 \leq n_0$, $1 \leq j_1 \leq n_1$, P_{i_0,i_1} are control points for $0 \leq i_0 \leq n_0$ and $0 \leq i_1 \leq n_1$, and $B_{i,0}^{(0)}(s)$, $B_{i,j}^{(0)}(s)$, $B_{i,0}^{(1)}(t)$ and $B_{i,j}^{(1)}(t)$ are polynomials in the B-spline. The polynomials are given as

$$B_{i,0}^{(0)}(s) = \begin{cases} 1, & s_i \leq s \leq s_{i+1} \\ 0, & otherwise \end{cases} \tag{A.2}$$

$$B_{i,j}^{(0)}(s) = \frac{(s - s_i)B_{i,j-1}^{(0)}(s)}{s_{i+j-1} - s_i} + \frac{(s_{i+j} - s)B_{i+1,j-1}^{(0)}(s)}{s_{i+j} - s_{i+1}} \tag{A.3}$$

$$B_{i,0}^{(1)}(t) = \begin{cases} 1, & t_i \leq t \leq t_{i+1} \\ 0, & otherwise \end{cases} \tag{A.4}$$

$$B_{i,j}^{(1)}(t) = \frac{(t - t_i)B_{i,j-1}^{(1)}(t)}{t_{i+j-1} - t_i} + \frac{(t_{i+j} - t)B_{i+1,j-1}^{(1)}(t)}{t_{i+j} - t_{i+1}} \tag{A.5}$$

B. Complete Bow Shape

This Appendix presents the optional MATLAB coding that can be added in the main file "runModel.m" in order to generate a complete bow shape together with the belonging m.-files. In addition, an illustration of the complete bow shape is found in this Appendix.

B.1 Optional MATLAB Coding

```matlab
% ------------ OPTIONAL: Includes the bottom of the bow ----------------
% Considering the whole bow shape by adding a mesh grid with control points.
% This option is only used for visualization.

% Additional input parameters
% -------------------------------------------------------------------------
% H_4            Additional height from z=0 to bottom of bow (-z) [m]
% phi1           Additional buttock angle 1                       [degree]
% phi2           Additional buttock angle 2                       [degree]
% phi3           Additional buttock angle 3                       [degree]
% -------------------------------------------------------------------------

H_4   = -4;
phi2  = 2;
phi3  = 6;
phi4  = 15;

% Generating additional control points for the parametric bow
[acpX,acpY,acpZ,am,an] = AdditionalCP(cpX,cpY,cpZ,H_3,phi,phi2,phi3,phi4);

% Weights of the control points
weights = ones(am,an);

% Defining coordinates within NURBS surface: (s,t)
ns = am*7; nt = an*7;
s = linspace(0,am-1,ns);
t = linspace(0,an-1,nt);

% Generating NURBS surface
[aX,aY,aZ] = SurfaceInterpolationGrid(acpX,acpY,acpZ,s,t,weights,degree);

% Plotting the additional grid of control points
AdditionalGridPlot(acpX,acpY,acpZ,an)
```

```matlab
% Scatter plotting of the additional control points
scatter3(acpX(:),acpY(:),acpZ(:),30,'k','filled')
scatter3(acpX(:),-acpY(:),acpZ(:),30,'k','filled')

% Creating three-dimensional shaded surface
hSurface = surf(aX,aY,aZ);
set(hSurface,'FaceColor',[0 0 0],'FaceAlpha',0.5);
hSurface = surf(aX,-aY,aZ);
set(hSurface,'FaceColor',[0 0 0],'FaceAlpha',0.5);
```

B.2 AdditionalCP.m

```matlab
% Adding points in the mesh grid to include the bottom of the ship.

function [acpX,acpY,acpZ,am,an] = AdditionalCP(cpX,cpY,cpZ,H_4,phi,phi2,...
    phi3,phi4)

an       = 4;
am       = 2;

x        = linspace(0,1,an);
z        = linspace(0,-1,am);

[acpX,acpZ] = meshgrid(x,z);
[acpY]     = zeros(am,an);


acpX(2,1) = cpX(1,1);
acpX(2,2) = cpX(1,2);
acpX(2,3) = cpX(1,3);
acpX(2,4) = cpX(1,4);
acpX(1,2) = cpX(1,2)-(-H_4/tand(phi));
acpX(1,3) = cpX(1,3)-(-H_4/tand(phi));
acpX(1,4) = cpX(1,4)-(-H_4/tand(phi));

% Set height in z-direction
acpZ(2,:) = cpZ(1,:);
acpZ(1,1) = H_4;

% Distance between CPs
ax12 = acpX(1,2)-acpX(1,1);
ax23 = acpX(1,3)-acpX(1,2);
ax34 = acpX(1,4)-acpX(1,3);

% Buttock angle
acpZ(1,2) = acpZ(1,1) + ax12*sind(phi2);
acpZ(1,3) = acpZ(1,2) + ax23*sind(phi3);
acpZ(1,4) = acpZ(1,3) + ax34*sind(phi4);

acpY(2,1) = cpY(1,1);
acpY(2,2) = cpY(1,2);
acpY(2,3) = cpY(1,3);
acpY(2,4) = cpY(1,4);

acpX = [acpX; cpX];
acpY = [acpY; cpY];
acpZ = [acpZ; cpZ];
[am,an] = size(acpX);

end
```

B.3   AdditionalGridPlot.m

```matlab
function AdditionalGridPlot(acpX,acpY,acpZ,an)

lw = 1;

%% Port side

hold on
for j=1:an
    % column wise line-plot
    plot3(acpX(:,j),acpY(:,j),acpZ(:,j),'--m','LineWidth',lw)
end

% for i=1:am
%     plot3(aX(i,:)', aY(i,:)',aZ(i,:)','--k','LineWidth',lw)
% end

% row wise line-plot
plot3(acpX(1,:),acpY(1,:),acpZ(1,:),'--m','LineWidth',lw)
plot3(acpX(2,:),acpY(2,:),acpZ(2,:),'--b','LineWidth',lw)



%% Starboard

hold on
for j=1:an
    plot3(acpX(:,j),-acpY(:,j),acpZ(:,j),'--m','LineWidth',lw)
end

% for i=1:am
%     plot3(aX(i,:)',-aY(i,:)',aZ(i,:)','--k','LineWidth',lw)
% end

plot3(acpX(1,:),-acpY(1,:),acpZ(1,:),'--m','LineWidth',lw)
plot3(acpX(2,:),-acpY(2,:),acpZ(2,:),'--b','LineWidth',lw)


end
```

B.4 Illustration of Complete Bow Shape
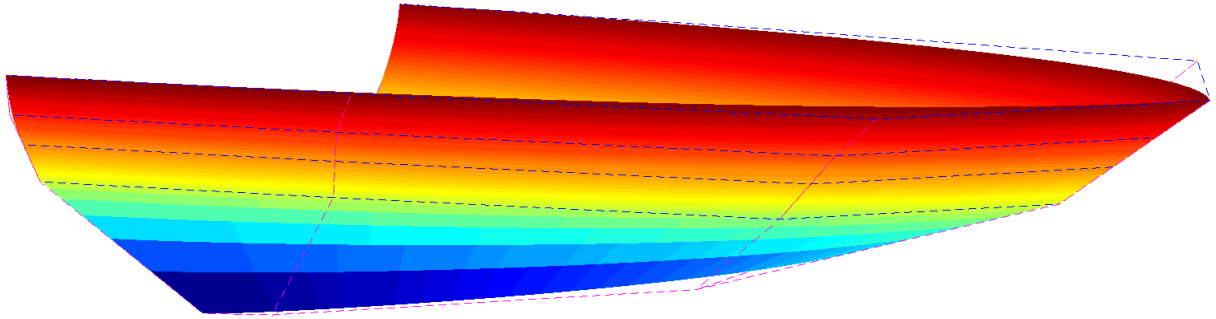
Figure B.1: Complete bow shape.

C. MATLAB code

The MATLAB coding is presented in this Appendix, which includes the main file and the belonging functions made for generating a 3D bow shape.

C.1   runModel.m

```matlab
% PARAMETRIC MODEL

% Input parameters
%-----------------------------------------------------------------------
% h_i          Ice thickness                                 [m]
% T_b          "Draught" - height from z=0 to ice top surface  [m]
% L_bow        Length of bow                                 [m]
% B            Breadth of ship                               [m]
% H_1          Height from z=0 to ice bottom surface         [m]
% H_2          Height from ice top surface to top of bow     [m]
% H_3          Height from z=0 to top of bow                 [m]
% c            Number of points along ice top surface within
%              x=0.001 and cpX(2:3,3)                        [-]
% d            Number of points along ice top surface within
%              cpX(2:3,3),cpX(2:3,4)-0.1                     [-]
% degree       Degree of polynomial function                [-]
% direction    Ray casting direction                        [-]
% phi          Buttock angle at stem (=stem angle)          [degree]
% alpha1       waterline entrance angle 1                    [degree]
% alpha2       waterline entrance angle 2                    [degree]
% beta1        Frame angle 1                                 [degree]
% beta2        Frame angle 2                                 [degree]
%
% n            Number of points in mesh grid, horizontal     [-]
% m            Number of points in mesh grid, vertical       [-]
% ns           Number of points on NURBS in s-direction      [-]
% nt           Number of points on NURBS in t-direction      [-]
% s            Array of points in s-direction on NURBS surface  [-]
% t            Array of points in t-direction on NURBS surface  [-]
%-----------------------------------------------------------------------

function runModel ()
clear all
close all
```

```matlab
%------------- Variables -------------
L_bow       = 27.24;
B           = 19.1;
alpha1      = 88;
alpha2      = 3;
beta1       = 80;
beta2       = 55;
phi         = 32;
h_i         = 0.75;
c           = 21;
d           = 19;


% ------------- Constants (should not be changed!) -------------
H_1         = 1;
H_2         = 1;
degree      = 3+1;
h           = 1e-4;
direction   = [0,1,0];



%% -------------------- Calling functions --------------------

% generate control points for parametric model
[cpX,cpY,cpZ,m,n,T_b] = ControlPoints(h_i,H_1,H_2,L_bow,B,alpha1,alpha2,...
    beta1,beta2,phi);

% additional nurbs surface parameter: weights of the control points
weights = ones(m,n);

% points along ice top surface
x_wl1 = linspace(0.001,cpX(3,3),c);
x_wl2 = linspace(cpX(3,3),cpX(3,4)-0.1,d);
x_wl = [x_wl1, x_wl2];
z_wl = ones(1,c+d)*T_b;
y_wl = zeros(1,c+d);

% find points on NURBS surface
[x_wl,y_wl,z_wl,s_wl,t_wl] = RayNurbsIntersection(cpX,cpY,cpZ,degree,...
    weights,x_wl,y_wl,z_wl,direction);

% compute normals on NURBS surface
[normalVector_wl,tangS,tangT] = SurfaceNormals(cpX,cpY,cpZ,degree,...
    weights,s_wl,t_wl,h);

% points along ice bottom surface
x_ice1 = linspace(0.001,cpX(2,3),c);
x_ice2 = linspace(cpX(2,3),cpX(2,4)-0.1,d);
x_ice = [x_ice1, x_ice2];
z_ice = ones(1,c+d)*(H_1);
y_ice = zeros(1,c+d);

% find points on NURBS surface
[x_ice,y_ice,z_ice,s_ice,t_ice] = RayNurbsIntersection(cpX,cpY,cpZ,...
    degree,weights,x_ice,y_ice,z_ice,direction);

% compute normals on NURBS surface
```

```matlab
[normalVector_ice,tangS,tangT] = SurfaceNormals(cpX,cpY,cpZ,degree,...
    weights,s_ice,t_ice,h);


%% -------------------- Results --------------------

% Displays the coordinates for the ice top waterline
% display(x_wl)
% display(y_wl)
% display(z_wl)

% % compute angles on ice top waterline
[alpha_wl, beta_wl, phi_wl, psi_wl, alpha_avg_wl,phi_avg_wl] ...
    = BowShapeAngles(normalVector_wl,c,d)

% Displays the coordinates for the ice bottom waterline
% display(x_ice)
% display(y_ice)
% display(z_ice)

% % compute angles on ice bottom waterline
[alpha_ice, beta_ice, phi_ice, psi_ice, alpha_avg_ice,phi_avg_ice]...
    = BowShapeAngles(normalVector_ice,c,d);


%% --------------------Plots--------------------

% coordinates within NURBS surface: (s,t)
ns = m*7; nt = n*7;
s = linspace(0,m-1,ns);
t = linspace(0,n-1,nt);

% generating NURBS surface
[X,Y,Z] = SurfaceInterpolationGrid(cpX,cpY,cpZ,s,t,weights,degree);

% plotting the grid of control points
GridPlot(cpX,cpY,cpZ,m,n)

% scatter plotting the control points
scatter3(cpX(:),cpY(:),cpZ(:),30,'k','filled')
scatter3(cpX(:),-cpY(:),cpZ(:),30,'k','filled')

% scatter3(x_wl,y_wl,z_wl,50,'k','filled')
% scatter3(x_ice,y_ice,z_ice,50,'k','filled')

% plotting normal vectors out from the NURBS surface
% quiver3(x_wl,y_wl,z_wl,normalVector_wl(:,1)',normalVector_wl(:,2)',...
%     normalVector_wl(:,3)','AutoScale','off','linewidth',2)
% quiver3(x_ice,y_ice,z_ice,normalVector_ice(:,1)',normalVector_ice(:,2)',..
%     normalVector_ice(:,3)','AutoScale','off','linewidth',2)

% creating three-dimensional shaded surface
hSurface = surf(X,Y,Z);
set(hSurface,'FaceColor',[0 0 0],'FaceAlpha',0.5);
hSurface = surf(X,-Y,Z);
set(hSurface,'FaceColor',[0 0 0],'FaceAlpha',0.5);
```

```matlab
xlabel('x')
ylabel('y')
zlabel('z')
axis('image')
view(90,90)
rotate3d on
hold off
box off

end
```

C.2   ControlPoints.m

```matlab
function [X,Y,Z,m,n,T_b] = ControlPoints(h_i,H_1,H_2,L_bow,B,alpha1,alpha2,...
    beta1,beta2,phi)

% Defining the amount of control points in the mesh grid
n       = 4;
m       = 4;

x       = linspace(0,1,n);
z       = linspace(0,1,m);
[X,Z]   = meshgrid(x,z);
[Y]     = zeros(m,n);

H_3     = H_1+h_i+H_2;
T_b     = H_1+h_i;
deltaH  = h_i+H_2;

% Set height in z-direction
Z(2,:) = H_1;
Z(3,:) = T_b;
Z(4,:) = H_3;

% Set bow length
X = X*L_bow;

% Set Breadth
Y(:,1) = B/2;

% Waterline entrance angle at exit
x12 = X(1,2) - X(1,1); % distance between CPs
Y(:,2) = B/2-sind(alpha2)*x12;
X(:,2) = X(:,1)+ cosd(alpha2)*x12;

% Waterline entrance angle at stem
x34 = X(1,4) - X(1,3);
radScale = 1.0;

x34 = x34*radScale;
```

```
Y(:,3) = sind(alpha1)*x34;
X(:,3) = X(:,4)- cosd(alpha1)*x34;

% Buttock angle
X(4,:) = X(4,:)*1.0;
X(3,:) = X(3,:)*(L_bow - H_2*tand(90-phi))/L_bow;
X(2,:) = X(2,:)*(L_bow - deltaH*tand(90-phi))/L_bow;
X(1,:) = X(1,:)*(L_bow - H_3*tand(90-phi))/L_bow;

% Frame angle
Y(4,:) = Y(4,:)*1.0;
Y(3,:) = Y(3,:)*(B/2 - H_2*tand(90-beta1))/(B/2);
Y(2,:) = Y(2,:)*(B/2 - h_i*tand(90-beta2))/(B/2);
Y(1,:) = Y(1,:)*(B/2 - T_b*tand(90-beta2))/(B/2);
end
```

C.3   BSplineBasis.m

```
% Generating the B-spline based on control points, knots and knot vector

% -----------------------------------------
% ncp       number of control points
% degree    degree of curve
% tknots    knot vector
% t         knots
% B         basis spline (polynomial)
% -----------------------------------------

function [B] = BSplineBasis(ncp,degree,t)
t0 = 0;
t1 = ncp-1.0;

tknots  = [ones(1,degree)*t0,linspace(0,3,ncp-2),ones(1,degree)*t1];

B = spcol(tknots,degree,t);
B = B(:,2:end-1);
end
```

C.4   SurfaceInterpolationGrid.m

```
% Generating NURBS surface by implementing the equations given for a
% polynomial surface

% --------------------------------------------------------------
% s         array of points in s-direction along NURBS surface
% t         array ofpoints in t-direction along NURBS surface
% ns        number of points on NURBS surface in s-direction
```

```matlab
% nt         number of points on NURBS surface in t-direction
% X2         array of x-coordinates of points in the st-plane on NURBS surface
% Y2         array of y-coordinates of points in the st-plane on NURBS surface
% Z2         array of z-coordinates of points in the st-plane on NURBS surface
% Bs         B-spline (polynomial) with reagrd to s
% Bt         B-spline (polynomial) with regard to t
% ------------------------------------------------------------
% The X2, Y2 and Z2 will represent the NURBS surface.

function [X2,Y2,Z2] = SurfaceInterpolationGrid(X,Y,Z,s,t,weights,degree)
[nx,ny] = size(X);

ns = length(s);
nt = length(t);

X2 = zeros(ns,nt);
Y2 = zeros(ns,nt);
Z2 = zeros(ns,nt);

Bs = BSplineBasis(nx,degree,s);
Bt = BSplineBasis(ny,degree,t);

sumWBB = zeros(ns,nt);
for ix=1:nx
    for iy=1:ny
        sumWBB = sumWBB + weights(ix,iy)*repmat(Bs(:,ix),1,nt)...
            .*repmat(Bt(:,iy)',ns,1);
    end
end

Rxy = zeros(ns,nt,nx,ny);
for ix=1:nx
    for iy=1:ny
        Rxy(:,:,ix,iy) = weights(ix,iy)*repmat(Bs(:,ix),1,nt)...
            .*repmat(Bt(:,iy)',ns,1)./sumWBB;
    end
end

for ix=1:nx
    for iy=1:ny
        tmp = Rxy(:,:,ix,iy);
        X2 = X2 + tmp*X(ix,iy);
        Y2 = Y2 + tmp*Y(ix,iy);
        Z2 = Z2 + tmp*Z(ix,iy);
    end
end
end
```

C.5   RayNurbsIntersection.m

```matlab
% This function is locating the points at the NURBS surface by intersecting
```

```matlab
% a shooting ray in y-direction from point p0 at the x-axis and the NURBS
% surface. The XA is to be minimized to zero to find the intersection of
% the points.

%---------------------------------------------------------------------
% nx        number of points in x-direction given by x0
% xT        array of x-coordinates of located points on NURBS surface
% yT        array of y-coordinates of located points on NURBS surface
% zT        array of z-coordinates of located points on NURBS surface
% sT        array of s-coordinates
% tT        array of t-corodinates
% p0        point at x-axis
% rst0      initial variable vector (ray)
% rst       variable vector (ray)
% x_0       located point on the NURBS surface
% Xst       array of x-coordinates of points in the st-plane on NURBS surface
% Yst       array of y-coordinates of points in the st-plane on NURBS surface
% Zst       array of z-coordinates of points in the st-plane on NURBS surface
% XA        vector pointing from a point on the NURBS surface towards the
%           the point on the ray
% ---------------------------------------------------------------------
function [xT,yT,zT,sT,tT] = RayNurbsIntersection(X,Y,Z,degree,weights,...
    x0,y0,z0,direction)

nx = length(x0);

xT = zeros(1,nx);
yT = zeros(1,nx);
zT = zeros(1,nx);

sT = zeros(1,nx);
tT = zeros(1,nx);

p0 = [x0(1),y0(1),z0(1)];

rst0 = [0,0,0];

for i=1:nx
    p0 = [x0(i),y0(i),z0(i)];
    F0 = @(rst) fun(rst,X,Y,Z,degree,weights,p0,direction);
    [rst,fval] = fminsearch(F0,rst0,optimset('TolX',1e-5));
    x_0 = p0+rst(1)*direction;
    sT(i) = rst(2);
    tT(i) = rst(3);
    xT(i) = x_0(1);
    yT(i) = x_0(2);
    zT(i) = x_0(3);
    rst0 = rst;
end
end

% Function computing points on the NURBS surface depending of control points
% X,Y,Z and the parameters s and t, which moves along the NURBS surface

function [normXA] = fun(rst,X,Y,Z,degree,weights,p0,direction)
```

```
[Xst,Yst,Zst] = SurfaceInterpolationGrid(X,Y,Z,rst(2),rst(3),weights,degree);
XA = p0+rst(1)*direction-[Xst,Yst,Zst];
normXA = norm(XA);
end
```

C.6   SurfaceNormals.m

```
% Generating normal vectors from the ice top waterline and the ice bottom
% surface by using central difference scheme

% ---------------------------------------------------------------
% n                 number of points in s-direction
% tangS,tangT       tangential direction with central difference
% normalVec         cross product of tangS and tangT
% h                 step size in central difference scheme
% sa, sb            resulting s-coordinates after introducing central
%                   difference
% ta, tb            resulting t-coordinates after introducing central
%                   difference
% ---------------------------------------------------------------

function [normalVec,tangS,tangT] = SurfaceNormals(CPx,CPy,CPz,degree,...
    weights,sT,tT,h)

n = length(sT);
normalVec = zeros(n,3);
tangS = zeros(n,3);
tangT = zeros(n,3);

for i=1:n
    sa = sT(i)-0.5*h;
    sb = sT(i)+0.5*h;
    s = sT(i);
    ta = tT(i)-0.5*h;
    tb = tT(i)+0.5*h;
    t = tT(i);

    [Psax,Psay,Psaz] = SurfaceInterpolationGrid(CPx,CPy,CPz,sa,t,weights,...
        degree);
    Psa = [Psax,Psay,Psaz];
    [Psbx,Psby,Psbz] = SurfaceInterpolationGrid(CPx,CPy,CPz,sb,t,weights,...
        degree);
    Psb = [Psbx,Psby,Psbz];
    [Ptax,Ptay,Ptaz] = SurfaceInterpolationGrid(CPx,CPy,CPz,s,ta,weights,...
        degree);
    Pta = [Ptax,Ptay,Ptaz];
    [Ptbx,Ptby,Ptbz] = SurfaceInterpolationGrid(CPx,CPy,CPz,s,tb,weights,...
        degree);
    Ptb = [Ptbx,Ptby,Ptbz];

    tangSab = Psb-Psa;
```

```matlab
    tangSab = tangSab/norm(tangSab);
    tangTab = Ptb-Pta;
    tangTab = tangTab/norm(tangTab);
    tangS(i,:) = tangSab;
    tangT(i,:) = tangTab;
    normalST = cross(tangSab,tangTab);
    normalVec(i,:) = normalST/norm(normalST);
end
```

C.7   BowShapeAngles.m

```matlab
function [alpha, beta, phi, psi, alpha_avg,phi_avg]...
    = BowShapeAngles(normalVector,c,d)
%% Computing bow angles

% waterline entrance angle
alphai = atand(normalVector(:,2)./normalVector(:,1));
alpha = 90-alphai;

% frame angle
beta = -atand(normalVector(:,2)./normalVector(:,3));

% buttock angle
phi = -atand(normalVector(:,1)./normalVector(:,3));

%flare angle
normalXY = normalVector;
normalXY(:,3) = 0;
chi = acosd(dot(normalVector,normalXY,2));
psi = 90-chi;


%% Computing average bow angles

% average waterline entrance angle
for i=1:c
    alphaI(i) = atand(normalVector(i,2)./normalVector(i,1));
    alpha_i(i) = 90-alphaI(i);
end

for j=1:d
    alphaII(j) = atand(normalVector(j+c,2)./normalVector(j+c,1));
    alpha_ii(j) = 90-alphaII(j);
end

alpha_avgI = mean(alpha_i(:));
alpha_avgII = mean(alpha_ii(:));
alpha_avg = (c*alpha_avgI+d*alpha_avgII)/(c+d);


% average buttock angle
```

```matlab
for i=1:c
    phiI(i) = -atand(normalVector(i,1)./normalVector(i,3));
end

for j=1:d
    phiII(j) = -atand(normalVector(j+c,1)./normalVector(j+c,3));
end

phi_avgI = mean(phiI(:));
phi_avgII = mean(phiII(:));
phi_avg = (c*phi_avgI+d*phi_avgII)/(c+d);


end
```

C.8   GridPlot.m

```matlab
function GridPlot(X,Y,Z, m,n)

lw = 1;

% point annotation (i,j)
% label = cell(n,m);
% for i=1:n
%     for j=1:m
%         label{i,j} = [' (' num2str(i) ',' num2str(j) ')'];
%     end
% end
% text(X(:),Y(:),Z(:),label(:),'HorizontalAlignment','right','FontSize',12);

%% Port side

hold on
for j=1:m
    % column wise line-plot
    plot3(X(:,j),Y(:,j),Z(:,j),'--r','LineWidth',lw)
end

for i=1:n
    % row wise line-plot
    plot3(X(i,:)',Y(i,:)',Z(i,:)','--b','LineWidth',lw)
end


%% Starboard

hold on
for j=1:m
    plot3(X(:,j),-Y(:,j),Z(:,j),'--r','LineWidth',lw)
end
```

```
for i=1:n
    plot3(X(i,:)',-Y(i,:)',Z(i,:)','--b','LineWidth',lw)
end

end
```

D. Convergence Study for Simulations

Table D.1: Convergence study for simulation step and length.

x_{step} [m]	x_{end} [m]	R_B [kN]
0.01	0.5	44
0.05	0.5	78
0.1	0.5	147
0.2	0.5	416
0.01	1.0	22
0.05	1.0	41
0.1	1.0	80
0.2	1.0	208
0.3	1.0	141
0.4	1.0	331
0.01	5.0	16
0.05	5.0	22
0.1	5.0	41
0.2	5.0	103
0.3	5.0	116
0.4	5.0	175
0.5	5.0	error
0.01	15.0	26
0.05	15.0	32

x_{step} [m]	x_{end} [m]	R_B [kN]
0.1	15.0	61
0.2	15.0	98
0.3	15.0	137
0.4	15.0	error
0.01	50.0	error
0.05	50.0	47
0.1	50.0	73
0.2	50.0	error
0.3	50.0	error
0.05	100.0	47
0.1	100.0	75
0.05	200.0	error
0.1	200.0	66
0.1	250	66
0.1	260	64
0.1	**265**	**64**
0.1	270	error

E. Simulation Results

Table E.1: Performed simulations for different bow shapes.

Bow shape	α_{avg} [degree]	ϕ_{avg} [degree]	R_B [kN]
1	21	28	26
2	37	29	18
3	36	44	29
4	37	20	17
5	23	41	46
6	40	38	26
7	40	27	22
8	48	24	23
9	25	26	20
10	26	20	15
11	25	32	26
12	25	38	34
13	23	34	31
14	24	22	16
15	28	31	28
16	29	19	16
17	28	25	21
18	27	36	37
19	32	18	14
20	31	30	26
21	31	36	40
22	36	22	22
23	37	31	20
24	36	38	24
25	36	41	29
26	23	39	41
27	31	37	42
28	31	27	27
29	32	24	24
30	31	34	37
31	36	33	25

Bow shape	α_{avg} [degree]	ϕ_{avg} [degree]	R_B [kN]
32	27	23	17
33	27	26	21
34	26	29	24
35	24	36	33
36	24	27	22
37	23	29	25
38	22	32	30
39	23	28	23
40	25	30	24
41	26	34	32
42	26	32	27
43	36	33	25
44	28	22	17
45	28	28	22
46	27	34	32
47	21	41	50
48	25	29	24
49	26	32	27
50	36	31	23